PHILOSOPHICAL TRANSACTIONS A

royalsocietypublishing.org/journal/rsta

Research

Cite this article: Grozeva NG, Klein F, Seewald JS, Sylva SP. 2020 Chemical and isotopic analyses of hydrocarbon-bearing fluid inclusions in olivine-rich rocks. *Phil. Trans. R. Soc. A* **378**: 20180431.
http://dx.doi.org/10.1098/rsta.2018.0431

Accepted: 30 October 2019

One contribution of 11 to a discussion meeting issue 'Serpentinite in the Earth system'.

Subject Areas:
geochemistry, oceanography

Keywords:
abiotic organic synthesis, methane, fluid inclusions, serpentinization, hydrothermal systems

Author for correspondence:
Niya G. Grozeva
e-mail: ngrozeva@alum.mit.edu

Electronic supplementary material is available online at https://doi.org/10.6084/m9.figshare.c.4748345.

THE ROYAL SOCIETY PUBLISHING

Chemical and isotopic analyses of hydrocarbon-bearing fluid inclusions in olivine-rich rocks

Niya G. Grozeva[1], Frieder Klein[2], Jeffrey S. Seewald[2] and Sean P. Sylva[2]

[1]Massachusetts Institute of Technology – Woods Hole Oceanographic Institution Joint Program in Oceanography, Cambridge, MA 02139, USA
[2]Department of Marine Chemistry and Geochemistry, Woods Hole Oceanographic Institution, Woods Hole, MA 02543, USA

NGG, 0000-0003-4582-9122

We examined the mineralogical, chemical and isotopic compositions of secondary fluid inclusions in olivine-rich rocks from two active serpentinization systems: the Von Damm hydrothermal field (Mid-Cayman Rise) and the Zambales ophiolite (Philippines). Peridotite, troctolite and gabbroic rocks in these systems contain abundant CH_4-rich secondary inclusions in olivine, with less abundant inclusions in plagioclase and clinopyroxene. Olivine-hosted secondary inclusions are chiefly composed of CH_4 and minor H_2, in addition to secondary minerals including serpentine, brucite, magnetite and carbonates. Secondary inclusions in plagioclase are dominated by CH_4 with variable amounts of H_2 and H_2O, while those in clinopyroxene contain only CH_4. We determined hydrocarbon abundances and stable carbon isotope compositions by crushing whole rocks and analysing the released volatiles using isotope ratio monitoring—gas chromatography mass spectrometry. Bulk rock gas analyses yielded appreciable quantities of CH_4 and C_2H_6 in samples from Cayman (4–313 nmol g^{-1} CH_4 and 0.02–0.99 nmol g^{-1} C_2H_6), with lesser amounts in samples from Zambales (2–37 nmol g^{-1} CH_4 and 0.004–0.082 nmol g^{-1} C_2H_6). Mafic and ultramafic rocks at Cayman exhibit $\delta^{13}C_{CH_4}$ values of −16.7‰ to −4.4‰ and $\delta^{13}C_{C_2H_6}$ values of −20.3‰ to +0.7‰. Ultramafic rocks from Zambales exhibit $\delta^{13}C_{CH_4}$ values of −12.4‰ to −2.8‰ and $\delta^{13}C_{C_2H_6}$ values of −1.2‰ to −0.9‰. Similarities in the carbon isotopic

compositions of CH_4 and C_2H_6 in plutonic rocks, Von Damm hydrothermal fluids, and Zambales gas seeps suggest that leaching of fluid inclusions may provide a significant contribution of abiotic hydrocarbons to deep-sea vent fluids and ophiolite-hosted gas seeps. Isotopic compositions of CH_4 and C_2H_6 from a variety of hydrothermal fields hosted in olivine-rich rocks that are similar to those in Von Damm vent fluids further support the idea that a significant portion of abiotic hydrocarbons in ultramafic-influenced vent fluids is derived from fluid inclusions.

This article is part of a discussion meeting issue 'Serpentinite in the Earth system'.

1. Introduction

Identifying sources and sinks for methane (CH_4) has remained one of the most important problems in hydrothermal research due to methane's numerous roles in the cycling of carbon, the evolution of microbial life and the limits of microbial life in extreme geochemical environments. Oxidation of abiotic CH_4 can represent a major source of metabolic energy for microbial organisms in diverse geological environments where mafic and ultramafic rock occur, including mid-ocean ridge and off-axis environments, passive margins, subduction zones, orogenic belts and ophiolites [1–5]. As serpentinization systems have existed throughout most of Earth's history, it is likely that such systems represent some of the most ancient microbial habitats on Earth (e.g. [6,7]). Indeed, the synthesis of abiotic hydrocarbons in serpentinization systems plays a central role in current hypotheses for the origin and early evolution of life on Earth (e.g. [8,9]) and possibly elsewhere in the solar system (e.g. [10,11]).

Seawater-derived hot-spring fluids at oceanic spreading centres are highly enriched in dissolved CH_4 relative to seawater, where $CH_{4(aq)}$ concentrations are typically below 2 nmol kg^{-1} [12]. In general, fluids that interact with ultramafic rocks contain aqueous CH_4 concentrations of the order of 2–3 mmolal [13–16], while those that interact with mafic rocks typically contain less than 1 mmolal $CH_{4(aq)}$ (e.g. [13]). Methane is also a common feature of continental ultramafic-influenced cold seep fluids, with some releasing reduced gases that contain up to 93% CH_4 by volume [17–19]. Previous studies have demonstrated that fluid inclusions are common in gabbroic rocks and are believed to represent a major reservoir of abiotic CH_4 in the lower oceanic crust [20–23]. Although it has long been postulated that such fluid inclusions may contribute to the inventory of CH_4 in ridge-crest hydrothermal fluids [21,24,25], more recent studies have provided compelling evidence for a direct link based on the chemical and isotopic composition of vent fluid CH_4 [16,26].

The purpose of this study was to characterize the chemical and isotopic compositions of low molecular weight hydrocarbons in fluid inclusions hosted in olivine-rich rocks, in order to facilitate a comparison to hydrocarbons venting from submarine hydrothermal systems and continental serpentinite-hosted gas seeps. To this end, we measured the relative abundances and carbon isotopic compositions of low molecular weight hydrocarbons in fluid inclusions hosted in mafic and ultramafic rocks from the Mount Dent oceanic core complex at the Mid-Cayman Rise (figure 1) and in ultramafic rocks from the Zambales ophiolite, Philippines (figure 2). The results allow constraints to be placed on the source of hydrocarbons in gas seeps at the Zambales ophiolite and in vent fluids emanating from the Von Damm hydrothermal field at Mount Dent, which have implications for the origin of abiotic CH_4 in other submarine and subaerial vent systems.

2. Material and methods

(a) Sample materials

Seven olivine-rich gabbroic and mantle rocks collected from the eastern flank of the Mount Dent oceanic core complex at the Mid-Cayman Rise (figure 1) using the deep submergence

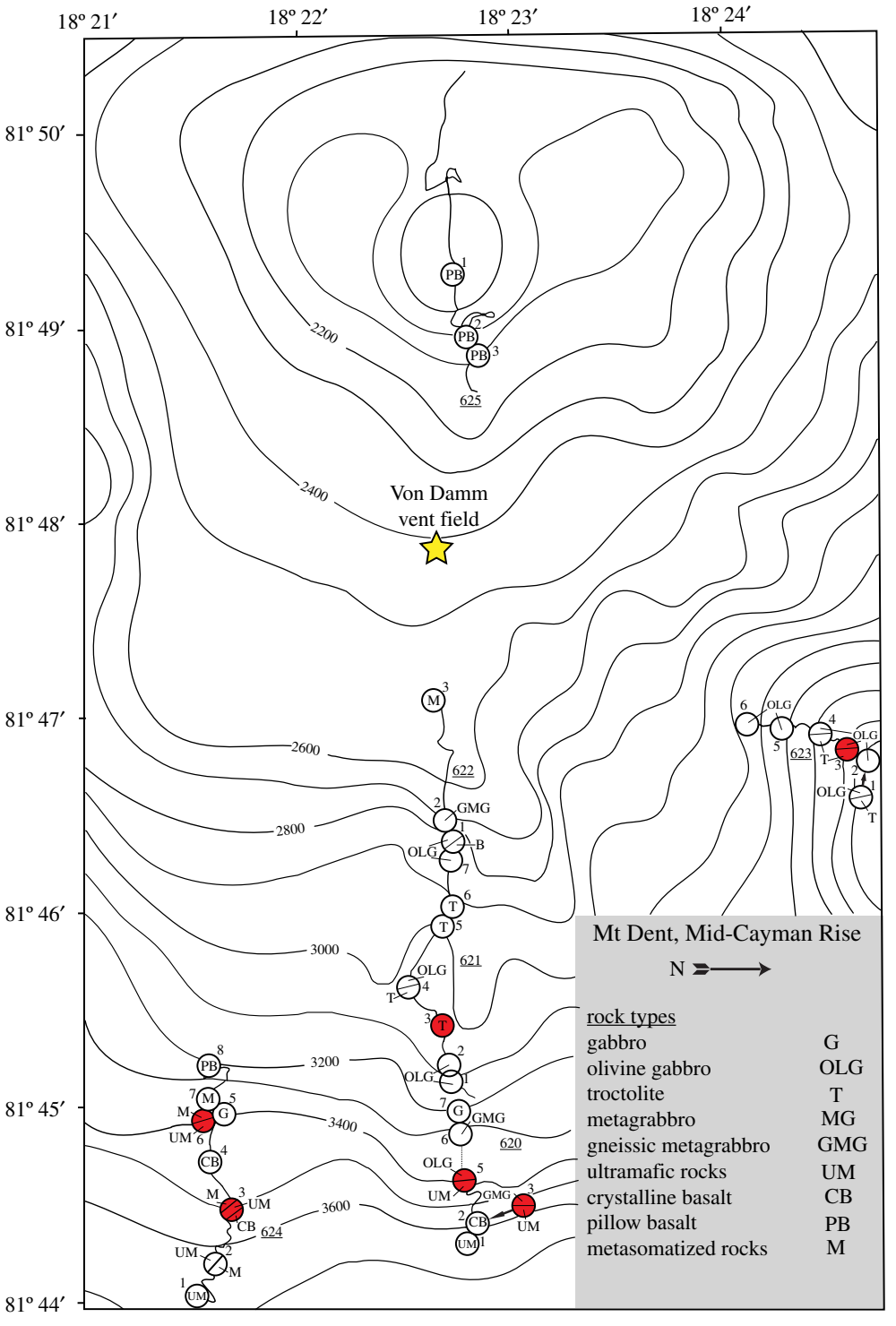

Figure 1. Bathymetric map of the eastern flank of the Mount Dent oceanic core complex on the Mid-Cayman Rise showing the locations of dive tracks and stations from the Cayman Trough Project. The distribution of rock types is shown for each numbered station. Samples used in this study are displayed as red circles. The approximate location of the Von Damm hydrothermal field (yellow star) is shown for comparison. Figure modified from Stroup & Fox [27]. (Online version in colour.)

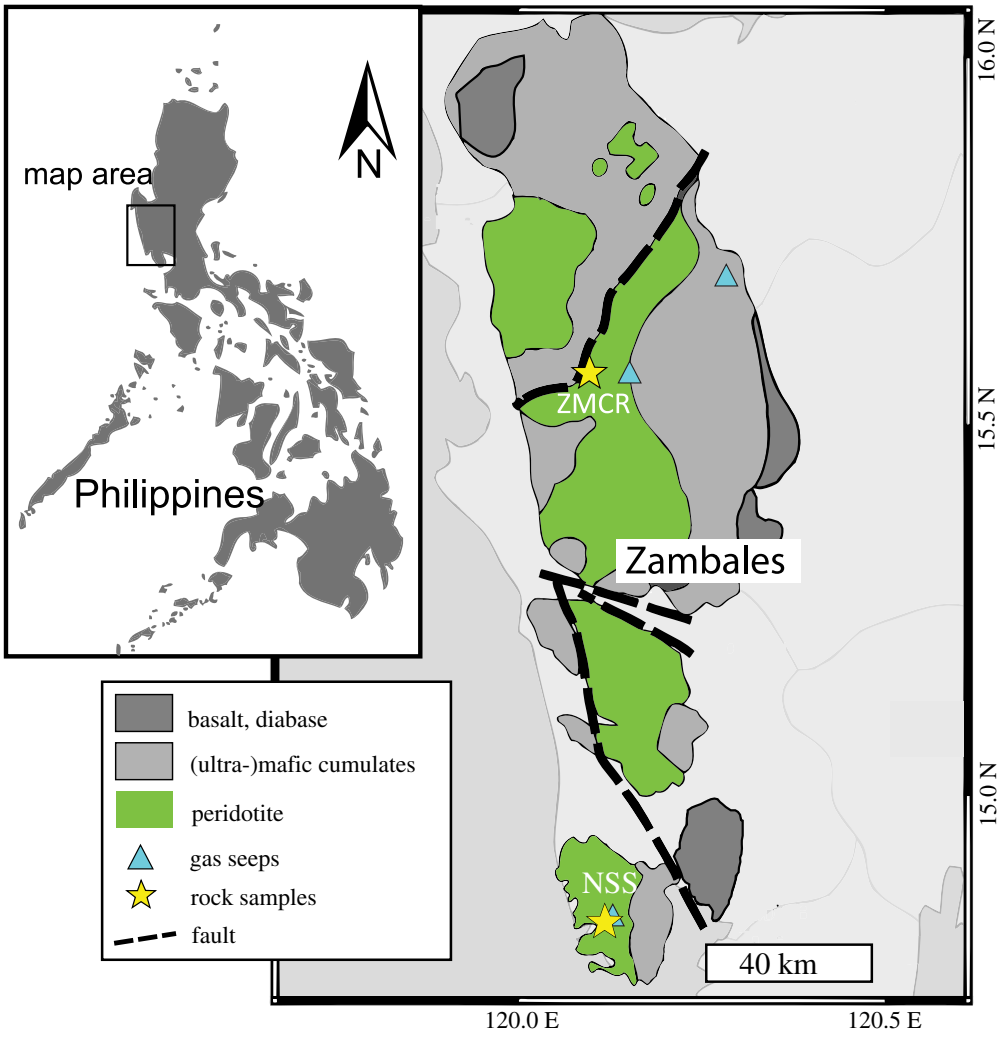

Figure 2. Map of the Zambales Ophiolite Complex in the Philippines displaying sampling locations and gas seeps. Figure modified from Dimalanta *et al*. [28] with gas seep GPS locations from Vacquand *et al*. [19]. (Online version in colour.)

vehicle *Alvin* in 1976 [27,29] were acquired from the Seafloor Samples Laboratory at Woods Hole Oceanographic Institution. The approximately 110 km long Mid-Cayman Rise is an ultraslow spreading centre (15–17 mm yr^{-1}) located between the Caribbean and the North American plates and is one of the deepest spreading centres worldwide [30]. The Mt Dent oceanic core complex, which rises approximately 3 km from the axial rift valley near the central portion of the Mid-Cayman Rise, has been exhumed by long-lived detachment faulting and hosts the Von Damm hydrothermal field [16,31–33]. Hydrothermal fluids venting at Von Damm are Mg- and SO_4-poor, and enriched in dissolved SiO_2, H_2, H_2S, CH_4 and C_2H_6, which is consistent with hydrothermal alteration of mafic (gabbro, diabase, basalt) and ultramafic (peridotite) rocks present at Mt Dent [27,34]. The rocks from the Mid-Cayman Rise examined here include one gneissic metagabbro, two olivine gabbros, two troctolites, one serpentinized spinel harzburgite and one serpentinized spinel lherzolite (table 1). Thin section petrography indicates that the harzburgite and lherzolite samples are 80% and 90% serpentinized, respectively. Olivine in the samples is primarily altered to serpentine and magnetite, while orthopyroxene is altered to serpentine, chlorite and minor talc. Cross-cutting veins composed of serpentine and magnetite

Table 1. Volatile and mineral contents of secondary inclusions determined from *in situ* Raman analyses. Normalized modes of primary minerals determined from visual estimates in thin section. Ant, antigorite; Brc, brucite; Cal, calcite; Cpx, clinopyroxene; Ctl, chrysotile; Dol, dolomite; Lz, lizardite; Mag, magnetite; Mg-Cal, high-Mg calcite; Mgs, magnesite; Oliv, olivine; Pg, paragonite; Plag, plagioclase; Sht, shortite; Tr-Act, tremolite-actinolite.

			composition of secondary inclusions in mineral hosts				normalized primary mode (vol.%)				
location	lithology	sample	olivine	plagioclase	clinopyroxene	hornblende	Plag	Oliv	Cpx	Opx	LOI (wt.%)
Cayman	gneissic metagabbro	ALV 620-3C	CH_4, H_2, Brc, Lz, Tlc	CH_4, H_2O, Pg	CH_4, Mg-Cal, Tr-Act	CH_4, Lz, Ant, Cal	—	—	—	—	1.497
	olivine gabbro	ALV 620-5-1	CH_4, H_2, Brc, Ctl, Lz, Ant, Mag, Dol	CH_4, H_2, H_2O, Pg, Cal, Sht?	CH_4, Tr-Act	—	75	5	20	0	1.695
		ALV 624-5-1	CH_4, H_2, Brc, Ctl, Lz, Mag, Mg-Cal	CH_4, H_2O, Cal	CH_4	—	50	35	15	0	1.394
	troctolite	ALV 621-3-1	CH_4, H_2, Brc, Ctl, Lz, Mag, Cal	CH_4, H_2, H_2O, Cal	—	—	80	20	0	0	3.464
		ALV 623-3-2	CH_4, H_2, Brc, Ctl, Lz, Ant, Mag, Cal, Dol, Mgs	CH_4, H_2, H_2O, Pg, Cal	CH_4, Tr-Act	—	90	9	1	0	0.985
	peridotite	ALV 624-3-3	CH_4, H_2, Brc, Ctl, Lz, Ant, Mag	—	—	—	0	85	1	14	10.40
		ALV 624-6-2	CH_4, H_2, Brc, Ctl	—	—	—	0	90	1	9	11.82
Zambales	dunite	ZMCR-02	CH_4, H_2, Brc, Ctl, Lz, Ant	—	—	—	0	99	1	0	13.49
		ZMCR-03	H_2, Brc, Ctl, Lz	—	—	—	0	99	1	0	13.72
	peridotite	NSS-02	CH_4, H_2, Brc, Lz, Ctl	—	—	—	0	88	2	10	3.657
		NSS-04	CH_4, H_2, Brc, Lz, Ctl, Ant, Dol	—	—	—	0	90	1	9	3.358

suggest the occurrence of multiple serpentinization events. More detailed descriptions of the mineralogical and chemical compositions of each sample are presented in previous studies [27,35,36].

Additional ultramafic rocks were collected from the Zambales ophiolite in the Philippines (figure 2), approximately 5 km from reported CH_4-rich gas seeps [17,19,37,38]. The Zambales ophiolite complex is part of a series of suprasubduction zone ophiolites at the western seaboard of the Philippine archipelago [39]. Its layered sequence consists of pillow lavas, sheeted dikes, gabbros, layered cumulates, transition zone dunites and residual peridotites, suggesting that it originated in magmatically robust oceanic crust, likely at a fast-spreading mid-ocean ridge [39]. Two partially serpentinized dunites were sampled at the Coto Mine, a chromite mine located in the Zambales Mineral Chromite Reservation in the Coto Block (N15°34′21.0″, E120°05′47.9″). The dunites are approximately 70% altered to a secondary mineral assemblage primarily composed of serpentine, brucite and trace quantities of magnetite and Ni-sulfides. Two serpentinized harzburgites were recovered from Nagsasa Cove in the San Antonio Massif, Philippines (N14°49′41.1″, E120°7′3.2″). These samples underwent approximately 20% serpentinization, resulting in the formation of serpentine, minor brucite and traces of micrometre-sized magnetite.

(b) Analytical methods

Thin sections of rock samples were examined with a petrographic microscope in transmitted and reflected light to document the types, sizes and distribution of fluid inclusions and their host mineralogy. A Horiba Jobin-Yvon LabRAM HR confocal Raman spectrometer with a 473 nm laser, 600 mm^{-1} grating, 100 µm confocal pinhole and 100 µm slit width was used to identify the volatile contents of individual inclusions and the mineralogy of inclusion walls. Quantitative CH_4 measurements were acquired using an 1800 mm^{-1} grating for improved spectral resolution. Spectra represent the average of at least three 30–120 s acquisitions typically conducted in the 150–2300 cm^{-1} and 2750–4400 cm^{-1} Raman shift regions. Estimates of CH_4 gas densities and pressures in fluid inclusions of select samples were determined from the measured Raman shift of the C–H symmetric stretching band relative to the band position of pure methane at 21°C and atmospheric pressure. Methane gas densities were calculated using the calibration of Zhang *et al*. [40], and CH_4 pressures were calculated using the calibration of Lu *et al*. [41].

Confocal Raman analysis requires a minimum fluid inclusion size of approximately 1 µm that depends on the inclusion depth and opacity of the host mineral. Detection limits for Raman spectroscopy are instrument-specific and depend on measurement conditions, which can vary from sample to sample and even within individual mineral grains. For instance, while it is possible to detect $CO_{2(g)}$ with a density of 0.001–0.002 g cm^{-3} in large (greater than 10 µm) fluid inclusions near the mineral surface [42–44], higher vapour densities are needed to detect $CO_{2(g)}$ in smaller inclusions or those buried deep in the mineral host. Wopenka & Pasteris [42] have reported detection limits for $CH_{4(g)}$ (0.0002 g cm^{-3}) and $H_{2(g)}$ (0.0001 g cm^{-3}) that are an order of magnitude lower than that for $CO_{2(g)}$. Although detection limits reported in the literature apply only to analytical conditions at the time of measurement, they are representative of typical sensitivity levels for the Raman spectroscopic techniques used in the present study.

The chemical and carbon isotopic compositions of volatile species contained within fluid inclusions were analysed by isotope ratio monitoring–gas chromatography mass spectrometry (irm-GCMS) following extraction of gases from fluid inclusions by mechanical crushing of whole-rock samples (figure 3). Unlike other extraction techniques, such as thermal decrepitation, crushing liberates gases only from inclusions and minimizes thermogenic formation of gases or thermal decomposition that can alter gas compositions and abundances [45–47]. In particular, thermal decrepitation methods have been shown to generate significant quantities of CO_2, CO and CH_4 by pyrolysis of high molecular weight organic material [45,48,49].

Whole-rock samples were cut into centimetre-sized pieces using a diamond-tipped blade, partially crushed using a tungsten-carbide jaw crusher, and then dry sieved to collect the 1–5 mm size fraction. Because olivine grains were partially altered in all samples, it was not feasible to

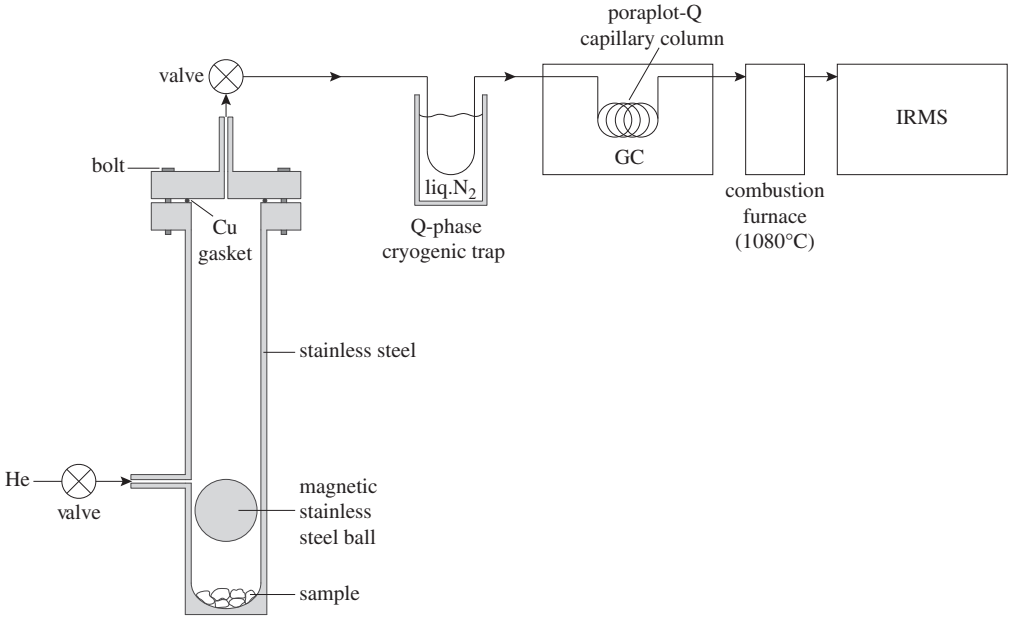

Figure 3. Schematic diagram of the stainless steel crushing device in line with an isotope ratio monitoring–gas chromatography mass spectrometry (irm-GCMS) system.

separate them from secondary mineral products and collect pure olivine separates. Therefore, only bulk rocks were analysed in this study. Gases were extracted from 1 to 5 mm whole-rock chips by placing a 1–4 g aliquot of each sample in a gas-tight, magnetically operated, stainless steel crushing device under an atmosphere of helium (figure 3). The crushing device was heated to 70°C during all steps of the analysis to reduce adsorption of gases onto mineral surfaces and facilitate their release into the carrier gas. After purging with helium to remove air, the crushing chamber was isolated from the He flow path using a valve, and a stainless steel ball inside the crushing device was manually raised and lowered 800 times using a magnet to pulverize the sample. After crushing, the chamber was sparged with He and the released volatiles were focused on a cryogenic trap immersed in liquid N_2. The cryogenic trap was interfaced directly to the irm-GCMS system for compositional and carbon isotopic analysis.

Crushing rocks in steel crushers is known to generate small amounts of gases, including H_2, CO, CH_4 and C_{2+} hydrocarbons by frictional heating during steel-to-steel contact [50–54]. Blank levels are reduced by the presence of sample material which can act as a cushion during contact between metal surfaces [53]. Blank experiments performed during this study revealed that moving the stainless steel ball up and down inside an empty crushing device continuously generated measurable quantities of CH_4 and C_2H_6. The level of hydrocarbon contamination was minimized by using a large sample size (1–4 g) to produce higher levels of sample-derived hydrocarbons and to cushion contact between the stainless-steel ball and inner walls of the chamber during crushing. Prior to analysing replicate aliquots of the same sample, the previously crushed aliquot was removed from the crushing device. Material that had adhered to the stainless-steel ball and the inside walls of the crushing device from a previous aliquot of the same sample was not removed in order to minimize steel-to-steel contact during subsequent crushing. Between analyses of different rock samples, the crushing device was scrubbed with a plastic brush to remove all rock powder, sonicated in water for 10 min and then dried in air at 60°C.

To quantify the blank, gases released during the crushing of two different blank materials were measured: (i) three previously pulverized samples (ALV 621-3-1, 623-3-2, 624-3-3) that were combusted in a muffle furnace at 1000°C in air for 24 h and (ii) 3 mm diameter combusted Pyrex

beads. The purpose of combusting the samples was to remove carbonate and organic carbon contaminants. A 2 g fraction of each blank material was crushed and analysed using the same procedure as described for the samples. Crushing of combusted Pyrex beads yielded CH_4 and C_2H_6 quantities of no more than 0.10 nmol g^{-1} and 0.0017 nmol g^{-1}, respectively (electronic supplementary material, table S1). This amount of CH_4 represents 0.02% of the CH_4 yield from the most CH_4-rich sample (ALV 620-3C) and 4% of the CH_4 yield from the least CH_4-rich sample (ZMCR-03). Ethane background levels represent 0.2% of the yield from the most C_2H_6-rich sample (ALV 620-3C) and 43% of the yield from the least C_2H_6-rich sample (ZMCR-02). For samples analysed for the carbon isotope composition of C_2H_6, the C_2H_6 blank represents 4% of the yield from the least C_2H_6-rich sample (ALV 623-3-2). The previously pulverized and combusted rock samples yielded C_2H_6 blank levels appreciably lower than those from the Pyrex beads and CH_4 blank levels comparable to those from the Pyrex beads, except for sample ALV 621-3-1 which released higher amounts of CH_4 (electronic supplementary material, table S1).

The abundance and carbon isotopic composition of CH_4 and C_2H_6 were determined using an irm-GCMS system consisting of an Agilent 6890 gas chromatograph coupled to a Thermo-Finnigan Delta Plus XL mass spectrometer through a Finnigan Gas Chromatograph Combustion Interface III held at 1080°C with a constant oxygen trickle. A Poraplot-Q capillary column was used to separate hydrocarbon compounds in the gas chromatograph. Stable carbon isotope values are reported in standard δ-notation relative to the Vienna Pee Dee Belemnite as follows:

$$\delta^{13}\mathrm{C}(‰) = \left[\frac{R_{\mathrm{spl}} - R_{\mathrm{std}}}{R_{\mathrm{std}}}\right] \times 1000, \tag{2.1}$$

where R_{spl} and R_{std} are the carbon isotope ratios ($^{13}C/^{12}C$) of the sample and standard, respectively. Average carbon isotope values and hydrocarbon abundances for each sample were obtained from analyses of two to five replicates of the bulk sample material.

Helium abundances and isotopic compositions were analysed by crushing in vacuum at the Isotope Geochemistry Facility at Woods Hole Oceanographic Institution. Whole-rock chips were dry sieved to collect the 1–2 mm size fraction. The chips were then sonicated in distilled water followed by acetone, and dried in a laminar flow hood under air. Approximately 0.3 g of sample was loaded into an ultra-high vacuum crusher [55] and crushed 20 times using a magnetic stainless steel piston. All He measurements were performed using a branch tube magnetic sector mass spectrometer, details of which are described in Kurz *et al.* [56]. Measured $^3He/^4He$ ratios are normalized to the atmospheric $^3He/^4He$ ratio, R_a (1.4×10^{-6}).

3. Results

(a) Distribution of secondary fluid inclusions

Secondary fluid inclusions in the samples occur as trails that extend along healed microfractures in minerals (figure 4) and across grain boundaries between adjacent minerals. Several generations of inclusion trails can be distinguished from cross-cutting relationships. Olivine contains the highest density of secondary fluid inclusions in all rock types. Olivine-hosted secondary fluid inclusions are particularly abundant in metagabbro, olivine gabbro and troctolite, with significantly fewer observed in peridotite and dunite. Individual inclusions range from less than 1 to 40 µm in diameter, with most inclusions being 1–15 µm in diameter. Plagioclase-hosted secondary fluid inclusions are typically smaller in size with diameters of 1–10 µm, but can range up to 25 µm in diameter, and are much less abundant than those in olivine. Inclusion trails within plagioclase are common in gabbro and troctolite, but rare in the gneissic metagabbro sample (ALV 620-3C) which exhibits strong alteration of plagioclase. By contrast, this sample contains abundant secondary inclusions in hornblende. Isolated inclusions of probable primary origin were detected in plagioclase but not in olivine. Few fluid inclusions are observed in clinopyroxene in any of the lithologies.

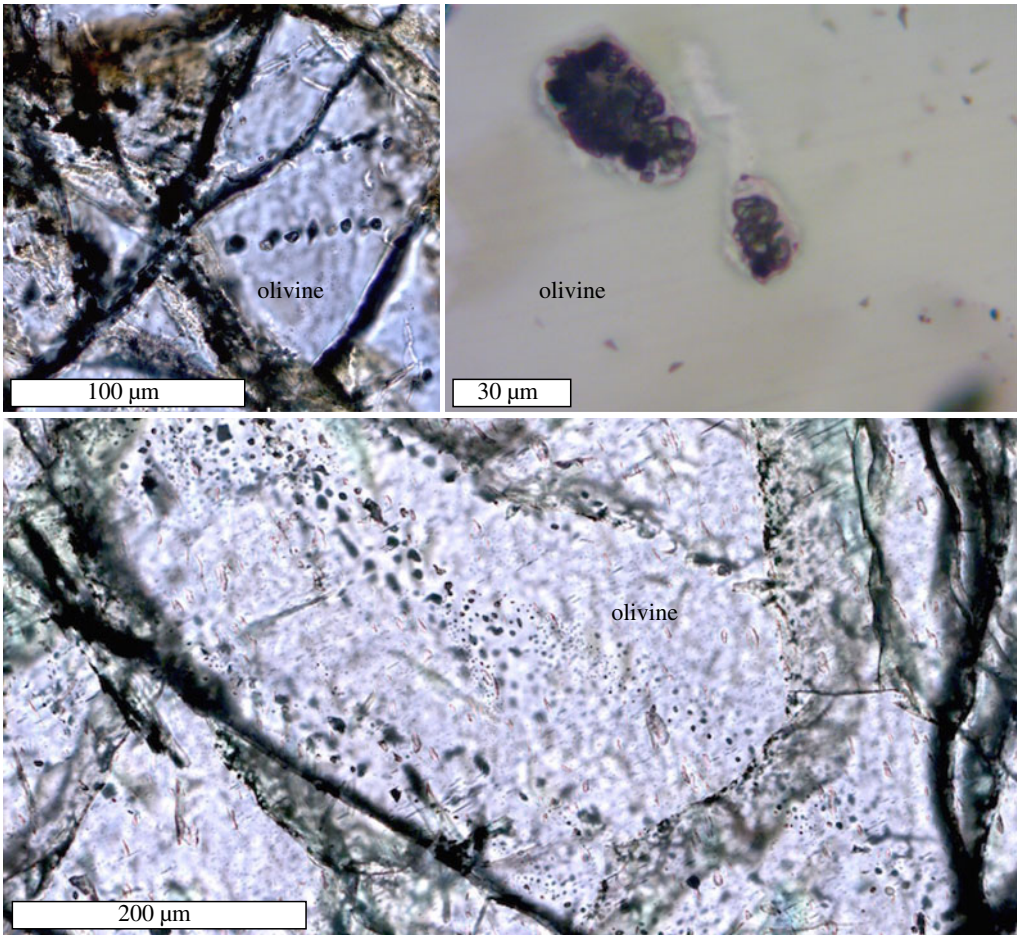

Figure 4. Representative thin section photomicrographs showing trails of CH_4-rich secondary fluid inclusions cross cutting olivine in troctolite from the Mid-Cayman Rise (Sample ALV 623-3-2; plane-polarized light). (Online version in colour.)

(b) Composition of secondary fluid inclusions

Olivine-hosted secondary fluid inclusions in all Cayman samples are dominated by CH_4, with minor H_2 (table 1; electronic supplementary material, figure S1). Carbon dioxide gas was not detected by Raman spectroscopy in any secondary inclusion in olivine. Preliminary data from sample ALV 624-3-3 indicate estimated CH_4 vapour densities of 0.16–0.29 g cm^{-3} and pressures of 20–54 MPa. Two-dimensional confocal Raman mapping shows abundant alteration minerals that typically occur as spatially discrete phases lining the inside walls and filling much of the interior of fluid inclusions (figure 5). Brucite and serpentine minerals, including chrysotile, lizardite and antigorite, are observed in olivine-hosted inclusions in all Cayman samples examined in this study. Magnetite and carbonate minerals, including calcite, high-Mg calcite, dolomite and magnesite, occur in olivine-hosted inclusions in most Cayman samples. No magnetite was detected in samples ALV 620-3C and 624-6-2, and no carbonates were detected in samples ALV 620-3C, 624-3-3 and 624-6-2. Free H_2O was not detected by Raman spectroscopy, either as a liquid or vapour phase, in any olivine-hosted secondary inclusion.

Secondary fluid inclusions in plagioclase are vapour- and liquid-rich, hosting gaseous CH_4 with variable amounts of liquid H_2O (figure 5, table 1 and electronic supplementary material, figure S2). Secondary inclusions in samples ALV 620-5-1, 621-3-1 and 623-3-3 also contain minor H_2. Calcite and paragonite are common daughter minerals in plagioclase-hosted secondary

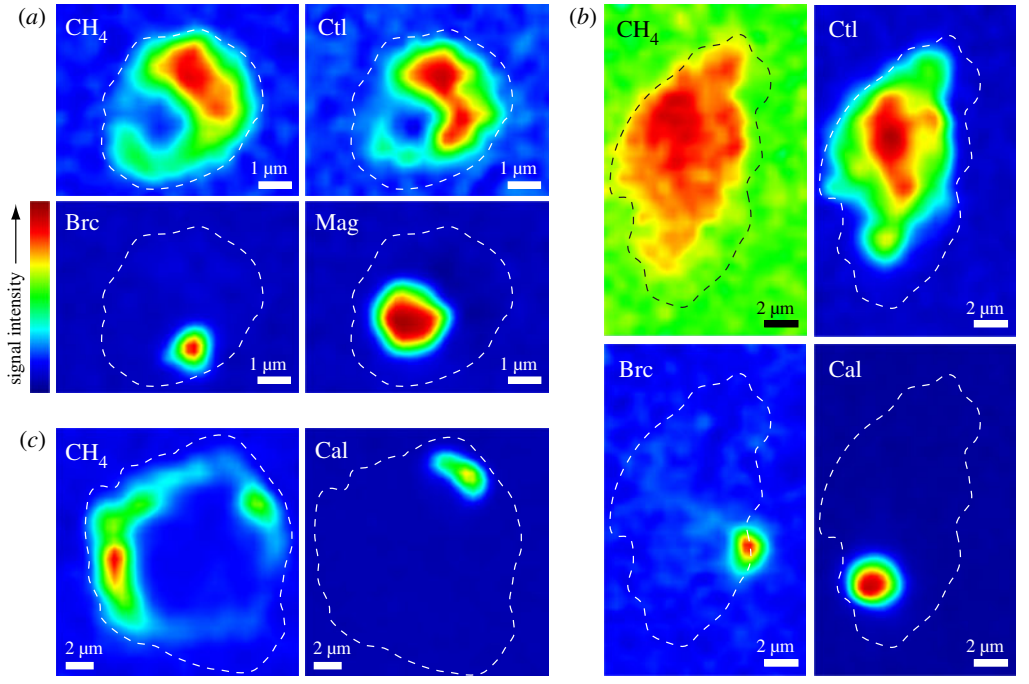

Figure 5. False-colour hyperspectral Raman maps showing the locations of mineral and gaseous species in secondary fluid inclusions hosted in olivine (*a*,*b*) and plagioclase (*c*) in Mid-Cayman Rise samples ALV 624-5-1 (*a*,*c*) and ALV 621-3-1 (*b*). Colours represent relative intensities of the characteristic Raman band for a particular phase, with warmer colours indicating higher signal intensities. Dashed lines represent the approximate outlines of the fluid inclusions. Brc, brucite; Cal, calcite; Ctl, chrysotile; Mag, magnetite. (Online version in colour.)

inclusions. Shortite [$Na_2Ca_2(CO_3)_3$], a sodium–calcium carbonate, was identified in Raman spectra of one plagioclase-hosted secondary inclusion in sample ALV 620-5-1.

Raman spectroscopy reveals that secondary fluid inclusions in clinopyroxene are vapour-dominated, with CH_4 as the sole volatile component (table 1 and electronic supplementary material, figure S3). High-Mg calcite was identified in the gneissic metagabbro sample ALV 620-3C. Tremolite-actinolite was detected in all samples, except ALV 624-5-1, on the basis of Raman band positions at 3677 cm^{-1} and 3662 cm^{-1} (electronic supplementary material, figure S3), with additional bands at lower wavenumbers (3645 cm^{-1}, 3626 cm^{-1}) occurring in some samples.

Olivine-hosted secondary fluid inclusions in ultramafic rocks from the Zambales ophiolite contain variable amounts of gaseous CH_4 and H_2 (table 1). Raman measurements reveal that H_2 is the dominant volatile component within olivine-hosted secondary inclusions in samples ZMCR-02 and ZMCR-03. Minor CH_4 was additionally detected in ZMCR-02, but was not detected in ZMCR-03. Samples NSS-02 and NSS-04, in contrast, host more abundant CH_4 with minor H_2. Raman data from olivine-hosted inclusions in NSS-04 yield estimated CH_4 vapour densities of less than or equal to 0.09 g cm^{-3} and pressures of up to 11 MPa. Olivine in all Zambales samples hosts brucite and serpentine minerals, including chrysotile, lizardite and antigorite. Dolomite was also detected in some olivine-hosted secondary inclusions in sample NSS-04.

(c) Hydrocarbon abundances and isotopes

(i) Hydrocarbon measurements

Chemical and carbon isotopic analyses of extracted hydrocarbon gases from whole-rock samples are displayed in table 2. Values reported for the abundance of individual hydrocarbons represent

minimum values as it is not possible to break open all inclusions through crushing. No correlations were observed between carbon isotopic compositions and hydrocarbon abundances or CH_4/C_2H_6 ratios. The measured $\delta^{13}C$ values of CH_4 were identical within analytical error (±0.5‰) for replicate analyses of the same sample. However, C_2H_6 was distinctly more ^{13}C-depleted in the first aliquot analysed for all samples, except for the most C_2H_6-rich sample, ALV 620-3C, which showed consistent $\delta^{13}C_{C_2H_6}$ values for replicate analyses. The remaining samples exhibited a trend toward more ^{13}C-enriched C_2H_6 with analysis of successive aliquots of sample material (electronic supplementary material, figure S4). Moving the stainless steel ball up and down inside an empty crushing device yielded $\delta^{13}C$ values for CH_4 (−36‰) and C_2H_6 (−29‰) that were significantly more negative than sample measurements, suggesting that the ^{13}C-depleted C_2H_6 observed in the first sample aliquots reflects contamination from the crushing device. Analysis of the first sample aliquot was conducted in a clean crushing device free of any rock powder, while analyses of subsequent aliquots were performed in a crushing device lined with previously pulverized sample material. A similar trend in CH_4 isotopic composition was not observed, likely because CH_4 concentrations are higher than those of C_2H_6.

The $\delta^{13}C_{C_2H_6}$ values for most samples from the Mid-Cayman Rise and Zambales ophiolite appeared to level off to within analytical error (±0.5‰) after analysis of the second or third aliquot of sample material (electronic supplementary material, figure S4). Average carbon isotope compositions of C_2H_6 in these samples were thus obtained from two to four successive analyses whose $\delta^{13}C_{C_2H_6}$ values are identical within analytical error (±0.5‰). However, the C_2H_6 isotopic compositions of two samples (ALV 624-5-1 and ALV 623-3-2) did not level off. Visual inspection revealed that these samples did not adhere well to the stainless steel surfaces of the crushing device during pulverization, likely resulting in higher levels of frictional heating and background hydrocarbon production during crushing. Therefore, C_2H_6 isotope compositions of samples ALV 624-5-1 and ALV 623-3-2 may be more affected by hydrocarbon contamination from the crushing device, and the measured $\delta^{13}C_{C_2H_6}$ values likely reflect minimum values. Samples ALV 624-5-1 and ALV 623-3-2 are characterized by very low degrees of alteration relative to the other samples. We speculate that the greater abundance of hydrous alteration minerals, including serpentine, talc and tremolite, in the more altered samples produces a 'stickier' rock powder that can adhere more effectively to the stainless steel walls of the crushing device, thus helping to minimize the production of background hydrocarbons by frictional heating.

(ii) Hydrocarbon compositions of Cayman and Zambales samples

The greatest absolute abundance of hydrocarbons in olivine-rich mafic and ultramafic rocks from the Mid-Cayman Rise is observed in sample ALV 620-3C, with average CH_4 and C_2H_6 contents of 313 nmol g^{-1} and 0.99 nmol g^{-1}, respectively, while the lowest quantity of hydrocarbons is observed in sample ALV 624-3-3, with average CH_4 and C_2H_6 contents of 4.3 nmol g^{-1} and 0.015 nmol g^{-1}, respectively (table 2). Most Cayman samples have CH_4/C_2H_6 ratios between 315 and 924. However, ALV 623-3-2 has a much higher CH_4/C_2H_6 ratio of 1372 relative to the other samples.

Methane in all Cayman samples shows a wide range of $\delta^{13}C$ values from −16.7‰ to −4.4‰ (table 2). Similarly, $\delta^{13}C$ values for C_2H_6 in most Cayman samples span a broad range from −20.3‰ to −10.6‰, except in sample ALV 620-5-1, which shows extremely ^{13}C-enriched C_2H_6 with a $\delta^{13}C_{C_2H_6}$ value of +0.7‰. Sample ALV 620-5-1 exhibits a trend toward more ^{13}C-enriched C_2H_6 with increasing number of crushes of the same sample aliquot, tentatively suggesting that there are distinct populations of fluid inclusions in the sample. However, no trend was evident in the CH_4 isotopic composition or CH_4/C_2H_6 ratio with cumulative number of crushes. Serpentinized peridotite samples from Cayman contained insufficient C_2H_6 for stable isotope measurements.

Serpentinized dunite and peridotite from the Zambales ophiolite also show a wide range of hydrocarbon abundances and carbon isotopic compositions (table 2). Samples NSS-02 and NSS-04 have higher average CH_4 contents (23–37 nmol g^{-1}) and C_2H_6 contents (0.075–0.082 nmol g^{-1})

Table 2. Average hydrocarbon abundances and carbon isotopic compositions in whole-rock samples from the Mid-Cayman Rise and the Zambales ophiolite. Here *n*, number of analyses; n.a., not analysed.

			CH_4						C_2H_6					CH_4/C_2H_6	
location	lithology	sample	Avg (nmol g^{-1})	2σ	*n*	Avg $\delta^{13}C$ (‰)	2σ	*n*	Avg (nmol g^{-1})	2σ	Avg $\delta^{13}C$ (‰)	2σ	*n*	Avg	2σ
Cayman	gneissic metagabbro	ALV 620-3C	313	23	6	−14.0	0.4	3	0.99	0.09	−12.5	0.4	4	315	28
	olivine gabbro	ALV 620-5-1	254	32	5	−4.4	0.3	3	0.68	0.05	+0.7	0.3	2	355	60
		ALV 624-5-1	93	5	5	−7.2	0.3	2	0.13†		−13.9†			676†	
	troctolite	ALV 621-3-1	78	9	7	−7.9	0.2	2	0.084	0.014	−10.6	0.1	2	924	9
		ALV 623-3-2	72	7	10	−16.7	0.3	3	0.047†		−20.3†			1372†	
	peridotite	ALV 624-3-3	4.3	1.1	2	−15.8	0.3	2	0.015	0.000	n.a.		2	350	10
		ALV 624-6-2	9.9	1.3	3	−11.6	0.6	3	0.020	0.003	n.a.		3	488	11
Zambales	dunite	ZMCR-02	2.0	0.3	2	−10.9	0.0	2	0.013	0.004	n.a.		2	163	33
		ZMCR-03	1.7	0.2	5	−12.4	1.5	5	0.004†		n.a.			431†	
	peridotite	NSS-02	23	2	5	−3.0	0.1	5	0.075	0.013	−0.9	0.2	3	327	56
		NSS-04	37	7	6	−2.8	0.0	2	0.082	0.010	−1.2	0.4	3	382	1

† $\delta^{13}C$ values of C_2H_6 and CH_4/C_2H_6 ratios represent minimum values due to contamination detected from the steel crusher. See text for details.

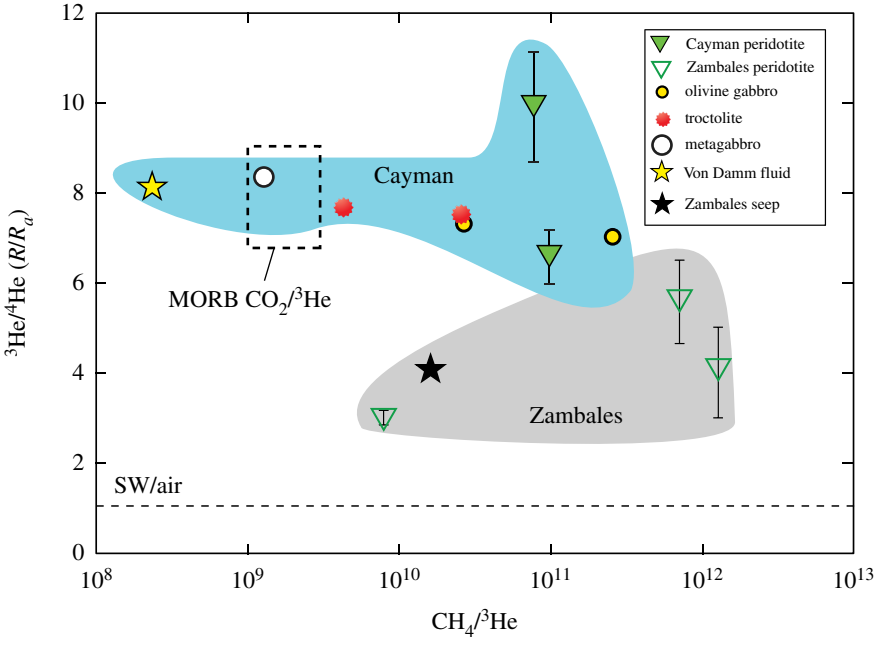

Figure 6. Plot of $^3He/^4He$ (R/R_a) versus $CH_4/^3He$ for whole-rock samples from the Mid-Cayman Rise and Zambales ophiolite. Except for the gneissic metagabbro sample, all samples exhibit $CH_4/^3He$ ratios that are significantly higher than the average $\Sigma CO_2/^3He$ ratio for mid-ocean ridge basalt (MORB). High $CH_4/^3He$ ratios may reflect inefficient helium extraction by crushing during the helium analyses or addition of He to the vent fluid from a source other than fluid inclusions. See text for discussion. (Online version in colour.)

relative to the more extensively serpentinized samples ZMCR-02 and ZMCR-03 (1.7–2.0 nmol g^{-1} CH_4 and 0.004–0.013 nmol g^{-1} C_2H_6). All samples show a relatively narrow range in average CH_4/C_2H_6 ratios from 163 to 431. Samples ZMCR-02 and ZMCR-03 exhibit $\delta^{13}C_{CH_4}$ values of −12.4‰ to −10.9‰. They contained insufficient C_2H_6 for stable isotope measurements. By contrast, samples NSS-02 and NSS-04 exhibit more ^{13}C-enriched CH_4, with $\delta^{13}C_{CH_4}$ values of −3.0‰ to −2.8‰. C_2H_6 in the NSS samples is slightly ^{13}C-enriched relative to CH_4 and shows average $\delta^{13}C_{C_2H_6}$ values of −1.2‰ to −0.9‰.

(d) Helium contents and isotopes

^4He contents of Mid-Cayman Rise samples exhibit a wide range from 4.7×10^{-7} to 9.0×10^{-11} cm^3 STP g^{-1} (table 3). Samples of serpentinized peridotite contain the lowest abundance of He, with ^4He contents that are one to two orders of magnitude lower than those in plutonic rock samples. With the exception of the highest He abundance in the gneissic metagabbro sample (ALV 620-3C), measured ^4He contents are 0.4–5 orders of magnitude lower than those reported for basaltic glasses from the Mid-Cayman Rise [57] (figure 6). Helium isotope compositions of most Cayman rocks fall within a relatively narrow range of 7.02–8.32 R_a, and are consistent with $^3He/^4He$ ratios documented in basaltic glasses from the Mid-Cayman Rise and other ocean ridges [57–59] (figure 6). Average $^3He/^4He$ ratios of 6.58 and 9.91 R_a for samples ALV 624-3-3 and 624-6-2, respectively, fall just outside this range, but have larger uncertainties owing to low He abundances in the samples.

Similar to serpentinized peridotite samples from the Mid-Cayman Rise, samples from the Zambales ophiolite have very low He abundances, with ^4He contents of 9.1×10^{-11} to 1.3×10^{-9} cm^3 STP g^{-1} (table 3). Average $^3He/^4He$ ratios range from 3.00 to 5.57 R_a and are lower than $^3He/^4He$ ratios in most of the Cayman samples, despite the larger uncertainties in the measured values.

Table 3. Helium in whole-rock samples from the Mid-Cayman Rise and the Zambales ophiolite. All measurements were performed by crushing in vacuum.

location	lithology	sample	crush ^{4}He (cc STP/g)	crush ^{4}He (nmol g^{-1})	^{3}He/^{4}He		$CH_4/^3$He
					(R/R_a)	2σ	
Cayman	gneissic metagabbro	ALV 620-3C	4.68×10^{-7}	2.09×10^{-2}	8.32	0.16	1.28×10^{9}
	olivine gabbro	ALV 620-5-1	2.26×10^{-9}	1.01×10^{-4}	7.02	0.24	2.56×10^{11}
		ALV 624-5-1	7.70×10^{-9}	3.44×10^{-4}	7.25	0.17	2.67×10^{10}
	troctolite	ALV 621-3-1	6.46×10^{-9}	2.88×10^{-4}	7.53	0.19	2.57×10^{10}
		ALV 623-3-2	3.53×10^{-8}	1.57×10^{-3}	7.66	0.15	4.27×10^{9}
	peridotite	ALV 624-3-3	8.97×10^{-11}	4.01×10^{-6}	9.91	1.23	7.70×10^{10}
		ALV 624-6-2	2.47×10^{-10}	1.10×10^{-5}	6.58	0.59	9.76×10^{10}
Zambales	dunite	ZMCR-02	1.33×10^{-9}	5.92×10^{-5}	3.00	0.16	8.06×10^{9}
	peridotite	NSS-02	9.12×10^{-11}	4.07×10^{-6}	5.57	0.92	7.23×10^{11}
		NSS-04	1.15×10^{-10}	5.11×10^{-6}	4.00	1.01	1.30×10^{12}

4. Discussion

(a) Formation and compositional evolution of carbon-rich fluid inclusions

The present study provides new constraints on the H_2, CH_4, C_2H_6 and alteration mineral contents of fluid inclusions in partially serpentinized peridotite and gabbroic rocks. These inclusions form when carbon-bearing aqueous fluids percolating in the lower lithosphere are trapped in primary minerals during healing of microfractures below the brittle–ductile transition temperature of the host mineral (less than 600–800°C for olivine; [60]). In mid-ocean ridge settings, trapped fluids likely represent seawater-derived fluids enriched in magmatic volatiles that circulated at depth close to the ridge axis, with CO_2 being derived from seawater, magmatic outgassing or both. Trapped water is likely seawater-derived since exsolution of volatiles from mid-ocean ridge basalt (MORB) magma produces chiefly CO_2 [61]. Owing to the strong temperature dependence of primary and secondary mineral stability during fluid–rock alteration, cooling of the trapped fluid and host mineral during exhumation creates a large thermodynamic drive for the aqueous alteration of the primary host mineral [23]. Olivine becomes thermodynamically unstable in the presence of water at temperatures below approximately 400°C and will react with water to form serpentine minerals, brucite, magnetite and $H_{2(g)}$ under closed-system conditions, according to the generalized serpentinization reaction [23,62–64]:

$$\text{olivine} + H_2O \rightarrow \text{serpentine} + \text{brucite} + \text{magnetite} + H_2. \tag{4.1}$$

The occurrence of reaction 4.1 at the scale of individual fluid inclusions that represent closed-system micro-reactors is indicated by the ubiquitous presence of serpentine, brucite, magnetite and H_2 within olivine-hosted fluid inclusions examined in this study (table 1; electronic supplementary material, figure S1).

The accumulation of H_2 during serpentinization has profound implications for carbon speciation in fluid inclusions due to the strong thermodynamic drive for the reduction of CO_2 to CH_4 and lesser quantities of C_{2+} alkanes via the general reaction

$$CO_2 + H_2 \rightarrow CH_4 + C_2H_6 + \cdots + H_2O, \tag{4.2}$$

at temperatures approximately below 350°C [65]. In addition to the formation of hydrocarbons, CO_2 may also be consumed by the precipitation of carbonate minerals that are observed in some

samples. Phase equilibria constraints indicate that carbonates can coexist in chemical equilibrium with CH_4 under a wide range of reducing conditions [66]. However, because the generation of H_2 in fluid inclusions depends on the oxidation of ferrous iron to ferric iron, the uptake of ferrous iron into the $FeCO_3$ component of carbonate minerals is expected to limit the amount of H_2 generated by serpentinization [67], thereby reducing the thermodynamic drive for hydrocarbon production [68]. The occurrence of Ca-bearing carbonates in olivine-hosted fluid inclusions in several samples suggests that circulating fluids contained dissolved Ca that was derived from seawater or from chemical interaction with Ca-bearing minerals in the surrounding rock.

The absence of free H_2O detected in secondary inclusions in olivine points to a complete or near-complete extent of serpentinization, resulting in the complete uptake of trapped H_2O into the hydrous minerals serpentine and brucite [23]. Furthermore, the lack of detectable CO_2 gas in olivine-hosted fluid inclusions suggests that all CO_2 was reduced to hydrocarbons or precipitated as carbonate minerals. Our observations contrast with previous findings of $CH_4 + CO_2 \pm H_2O$-bearing fluids in olivine-hosted inclusions in Southwest Indian Ridge (SWIR) gabbroic rocks [20,21], whose compositions suggest disequilibrium between trapped volatiles and the olivine host [23].

Unlike olivine, plagioclase is Fe-poor and equilibration with trapped fluid during cooling may yield limited amounts of H_2 from ferrous iron oxidation. Accordingly, the presence of H_2 and CH_4 in plagioclase-hosted inclusions in some Cayman samples (table 1; electronic supplementary material, figure S2) suggests that requisite H_2 for CO_2 reduction to CH_4 was derived from a source external to the fluid inclusion or generated *in situ* by radiolysis due to the decay of radiogenic elements in plagioclase. Although H_2 was not detected in any clinopyroxene-hosted secondary fluid inclusion, H_2 may have been present at a level below the detection limit of Raman spectroscopy, or may have been completely consumed by CO_2 reduction to CH_4 (table 1; electronic supplementary material, figure S3). Generation of H_2 within clinopyroxene-hosted inclusions may occur by oxidation of ferrous iron initially present in clinopyroxene to ferric iron in tremolite-actinolite; however, the amount of H_2 that can be generated by this mechanism is limited due to the low ferric iron contents generally observed in tremolite-actinolite [69]. The possibility also exists that either H_2 or CH_4 in clinopyroxene-hosted inclusions may have been externally derived.

(i) Sources of helium and carbon in secondary fluid inclusions

At the Mid-Cayman Rise, $^3He/^4He$ ratios in lower crustal plutonic and mantle rock samples vary from 6 to 10 R_a (figure 6) and are consistent with a mantle source for helium. ^4He abundances in Cayman samples are approximately 1–5 orders of magnitude lower than those in MORB from fast-spreading ocean ridges [70] and may reflect the magma-poor source region of the ultraslow-spreading Mid-Cayman Rise or loss of ^4He during rock alteration. At Zambales, $^3He/^4He$ ratios of 3.0–5.6 R_a in olivine-rich rocks examined in this study are significantly lower than those typically in the mantle as exemplified by MORB (7–9 R_a). These low $^3He/^4He$ ratios likely reflect the addition of radiogenic ^4He from U-Th decay in the ultramafic protolith [17,19].

The isotopic composition of CH_4 trapped within fluid inclusions in olivine-rich rocks from the Mid-Cayman Rise and Zambales ophiolite is characterized by a large range of $\delta^{13}C$ values that varies from −16.7 to −2.8‰. The more positive end of this range directly overlaps with the isotopic composition of mantle-derived CO_2 (figure 7), consistent with CH_4 formation from a mantle carbon source. Samples that contain CH_4 that is more depleted in ^{13}C than mantle-derived CO_2 are consistent with isotopic fractionation during CH_4 formation. The extent of isotopic fractionation during CO_2 reduction to CH_4 is dependent on several factors, including formation temperature, partitioning of carbon among different species, such as CO_2, CH_4, C_{2+} alkanes and carbonate minerals, and the presence of an open or closed chemical system. Partial reduction of CO_2 to hydrocarbons under hydrothermal conditions generates CH_4 and C_{2+} alkanes that are depleted in ^{13}C relative to the initial CO_2 source [83–86]. For example, equilibrium $^{13}C/^{12}C$ fractionation factors ($1000\ln\alpha$) between dissolved CO_2 and CH_4 are −30 and −18 at 200°C and

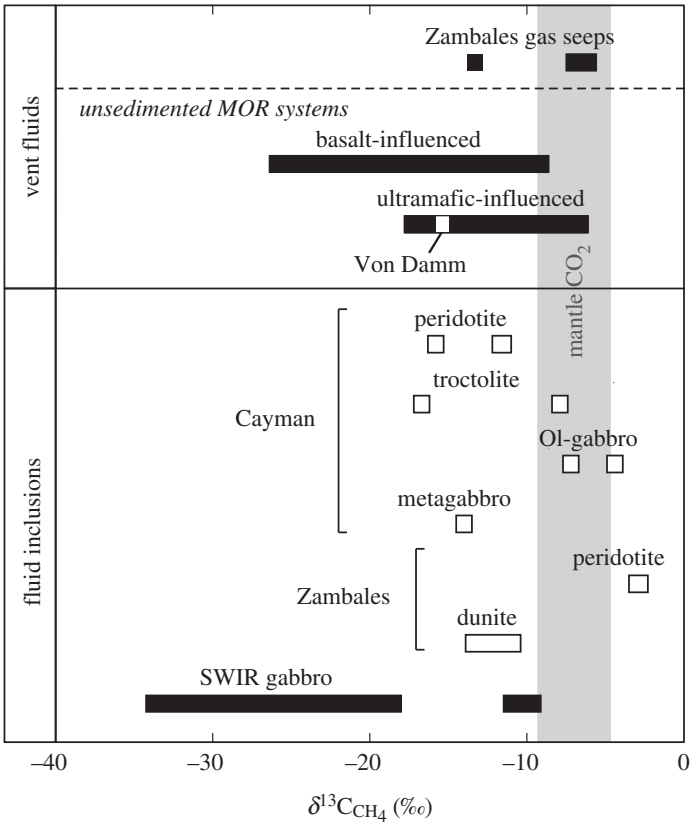

Figure 7. Ranges in carbon isotopic compositions of CH_4 from whole-rock samples in this study, Zambales gas seeps, mid-ocean ridge (MOR) vent fluids and Southwest Indian Ridge (SWIR) gabbros. $\delta^{13}C_{CH_4}$ values in mafic and ultramafic rocks from Cayman encompass the $\delta^{13}C$ value of dissolved CH_4 in Von Damm endmember fluids (−15.4‰), suggesting that CH_4 budgets at Von Damm may be influenced by interaction with olivine-rich rocks in the subsurface. $\delta^{13}C$ values of CH_4 issuing from Zambales gas seeps at Los Fuegos Eternos (−7.0 ± 0.4‰) and Nagsasa (−5.6‰) lie in between the ranges of $\delta^{13}C_{CH_4}$ in serpentinized dunite and peridotite from the ophiolite, suggesting that CH_4 gas in Zambales may be sourced from these two rock types. See text for discussion. Data are from [13,14,16,17,19,21,22,71–82].

300°C, respectively [84]. Generation of CH_4 with mantle $\delta^{13}C$ values (−10‰ to −4‰) from magmatic CO_2 thus suggests the near-quantitative reduction of CO_2 to CH_4 in a closed system, consistent with the lack of detectable CO_2 in fluid inclusions. Assuming the fluid inclusion remains a closed system, CH_4 with a $\delta^{13}C$ value that is significantly more negative than −10‰ points to the incomplete reduction of magmatic CO_2 to CH_4.

Previous studies have examined the chemical and isotopic compositions of CH_4-rich fluid inclusions in gabbroic rocks from the ultraslow-spreading SWIR and Mid-Cayman Rise [20–22]. Comparison of the concentrations of CH_4 extracted from fluid inclusions in this study (1.7–313 nmol g^{-1}) with concentrations of CH_4 released from SWIR gabbros during thermal decrepitation (120–2900 nmol g^{-1}) [21,22] indicates generally higher values in the SWIR samples with some degree of overlap. The majority of SWIR samples are characterized by $\delta^{13}C_{CH_4}$ from −34.2‰ to −18.0‰, with two samples exhibiting more positive $\delta^{13}C$ values of −11.5‰ and −9.1‰ [20–22]. Isotopic analysis of bulk carbon in the Mid-Cayman Rise samples by elemental analysis combined with isotope ratio mass spectrometry (EA-IRMS) indicates values that vary from −26.7‰ to −23.6‰ [22]. With the exception of the two most positive values, $\delta^{13}C$ values for CH_4 in SWIR gabbros and for bulk carbon in Mid-Cayman Rise gabbros are significantly more negative than $\delta^{13}C_{CH_4}$ values of −16.7‰ to −2.8‰ measured in plutonic rocks during this study (figure 7).

Isotopic analyses of CH_4 in SWIR gabbros were performed by step-heating of the samples to 450–500°C and greater than 900–1000°C in the absence of O_2 to decrepitate fluid inclusions and release trapped gases; EA-IRMS used for bulk carbon analysis of the Mid-Cayman Rise gabbros involved combusting samples at 1060°C [21,22]. In the case of the SWIR analyses, heating at these temperatures in the absence of O_2 can generate CH_4 by pyrolysis of organic carbon material, which can represent a variable but significant portion of the total carbon content of fresh and altered igneous rocks. For example, studies of basaltic glass and mantle xenoliths demonstrate the occurrence of condensed carbonaceous material as films and discrete particles along crack surfaces, grain boundaries and fluid inclusion walls, with bulk $\delta^{13}C$ values of −29‰ to −22‰ [87–93]. Gabbroic and ultramafic rocks in altered oceanic crust contain variable but significant quantities of organic carbon, up to 7000 ppm, with a similar range in carbon isotopic compositions [94–97]. Thus, it is highly likely that heating of the SWIR samples to decrepitate fluid inclusions resulted in the pyrolysis of higher molecular weight organic compounds and the generation of ^{13}C-depleted CH_4. Accordingly, the carbon isotopic compositions of CH_4 reported for SWIR gabbros [21,22] likely include a contribution of pyrolytic CH_4, resulting in $\delta^{13}C_{CH_4}$ values that are more negative than those of CH_4 released from fluid inclusions in this study.

(b) Implications for the origin of methane in hydrothermal fluids and gas seeps

(i) Ridge-crest hydrothermal fluids

The existence of abundant CH_4-bearing fluid inclusions in rocks that compose a major fraction of the oceanic lithosphere has potential implications for the chemical composition of fluids venting from axial hot springs. Convective circulation of hot and highly reactive aqueous fluids in the crust may release volatiles trapped in fluid inclusions through dissolution of their mineral hosts during hydrothermal alteration and weathering. Fracturing of the olivine host likely represents an additional mechanism to release volatiles from fluid inclusions. The contribution of fluid inclusions to the chemical inventory of ridge-crest hydrothermal fluids can be assessed by examining the composition of vent fluids at the Von Damm hydrothermal field situated on the southern flank of the Mt Dent oceanic core complex at the Mid-Cayman Rise [31,32], in close proximity to the sampling locations of rocks analysed during this study (figure 1). Hydrothermal activity at the Von Damm vent field involves the venting of near neutral $pH_{(25°C)}$ fluids at temperatures up to 226°C [16]. Endmember vent fluids are highly reducing, with dissolved H_2 concentrations of 18.2 mmol kg^{-1}, and contain substantial quantities of dissolved CH_4 (2.81 mmol kg^{-1}), C_2H_6 (639 nmol kg^{-1}) and C_3H_8 (56 nmol kg^{-1}) [16]. Based on the observation that CH_4 in the Von Damm vent fluids contained radiocarbon (^{14}C) at the limit of detection, while dissolved ΣCO_2 contained five times more ^{14}C, McDermott *et al*. [16] concluded that carbon in CH_4 was not derived from dissolved CO_2 in convecting seawater-derived hydrothermal fluids. Additional evidence to support this assertion was provided by the concentration and stable carbon isotope composition of vent fluid ΣCO_2, which was identical to that in the seawater source fluid, indicating that there had been no ΣCO_2 addition or consumption during hydrothermal circulation. Collectively, these observations led McDermott *et al*. [16] to postulate that CH_4 and possibly other low molecular weight hydrocarbons in the Von Damm vent fluids were leached from fluid inclusions in deep-seated reaction zones during hydrothermal circulation.

Leaching of CH_4 and other hydrocarbons from fluid inclusions represents a fundamentally different process than paradigms for CH_4 formation that involve the reduction of dissolved CO_2 during convection of seawater-derived fluids in the crust. Stable isotope, radiocarbon and mass balance constraints at the Von Damm hydrothermal field indicate that abiotic CH_4 formation does not occur in actively circulating fluids beneath Mt Dent [16]. This suggests that insufficient time is available to surmount the large kinetic barriers inhibiting CO_2 reduction to CH_4 under hydrothermal conditions [64,67,98–101]. Estimated crustal residence times of less than 3–10 years for high-temperature (greater than 200°C) ridge-crest hydrothermal fluids [102,103] and hundreds to 10 000 years for lower temperature ridge flank hydrothermal fluids [104–106] suggest that

even longer reaction times may be necessary to generate significant quantities of abiotic CH_4 from CO_2 during active fluid convection. However, longer reaction times can be achieved by trapping volatiles within fluid inclusions in lower crustal plutonic and mantle rocks. Constraints from thermochronology indicate that rocks exhumed along oceanic detachment faults take 0.3–0.7 Ma to cool from approximately 850°C to 200°C [107–111]. Exhumation by detachment faulting involves horizontal motion (off-axis, at a rate that is roughly half of the spreading rate; [112]) in addition to approximately 5–10 km of vertical motion [113]. Detachment faults are known to steepen with depth at the ridge axis (e.g. [114,115]), which means that a significant portion of the cooling time of an inclusion-bearing rock can be spent moving mostly upwards in the near-axis domain. This may provide sufficient time for the reduction of CO_2 to CH_4 to occur in fluid inclusions while the host rock remains close to the spreading axis. For instance, that could be the case at the near-axis Logatchev hydrothermal site on the Mid-Atlantic Ridge. By contrast, host rocks can move farther off-axis in less magma-rich regions of spreading centres where more extension is accommodated through slip on detachment faults, as may be the case for the off-axis Von Damm and Lost City sites. In both cases, carbon-rich fluid inclusions may persist in the subsurface of oceanic core complexes for hundreds of thousands of years before extraction by circulating seawater-derived fluids, which may allow sufficient time for the reduction of dissolved CO_2 to CH_4 and other low molecular weight hydrocarbons.

Aqueous CH_4 in the Von Damm vent fluids has a $\delta^{13}C$ value of −15.4‰, which falls within the range of $\delta^{13}C_{CH_4}$ values measured in mafic and ultramafic rocks from the Mt Dent oceanic core complex of −16.7‰ to −4.4‰ (figure 7). Similarly, the range of $\delta^{13}C_{C_2H_6}$ values in the Cayman rock samples (−20.3‰ to −10.6‰), with the exception of ALV 620-5-1 (+0.7‰), encompasses the $\delta^{13}C$ value of −12.7‰ for aqueous C_2H_6 in the Von Damm vent fluid (figure 8). Moreover, $^3He/^4He$ ratios of 6.58–9.91 R_a in Cayman rocks all show mantle-like values within analytical error (figure 6) and are consistent with the average $^3He/^4He$ ratio (8.14 ± 0.13 R_a) in Von Damm hydrothermal fluids [16]. The similarities in the carbon and He isotopic compositions between Von Damm fluids and Cayman rocks are consistent with a model in which hydrocarbons and helium in Von Damm fluids may be derived by leaching of volatiles trapped within subsurface olivine-rich rocks.

While hydrocarbon isotopic compositions in vent fluid and fluid inclusions show a high degree of overlap, the molar CH_4/C_2H_6 ratios of 315–1372 measured in Cayman rocks are significantly lower than the Von Damm endmember fluid ratio of 4397 [16] (figure 9). Differences in CH_4/C_2H_6 ratios between the rocks and fluids may reflect the decomposition of C_{2+} hydrocarbons during transport in the Von Damm hydrothermal fluids at elevated temperatures. Laboratory hydrothermal experiments have demonstrated relatively rapid oxidative degradation of C_{2+} hydrocarbons in the presence of Fe-sulfide and oxide minerals that buffer the redox state to conditions analogous to ridge-crest hydrothermal systems [116]. Experimentally determined half-lives of C_2H_6 by oxidative decomposition at 300–350°C are on the order of a few months [116], and are shorter than residence times of less than 3–10 years estimated for actively convecting high-temperature fluids in submarine hydrothermal systems [102,103].

Rocks from the Mid-Cayman Rise, except for sample ALV 620-3C, exhibit $CH_4/^3He$ ratios significantly higher than the Von Damm vent fluid ratio of 2.34×10^8, indicating the addition of carbon or loss of helium in the rocks (figure 6). Several factors may account for such higher ratios, in particular the different methodologies used to analyse hydrocarbon and helium contents. Hydrocarbon abundances were measured by crushing whole-rock samples 800 times each, whereas He contents were measured by crushing whole-rock samples only 20 times each, likely resulting in more incomplete rupturing of fluid inclusions. Furthermore, vacuum crushing and melting experiments demonstrate that the majority (79–95%) of helium in oceanic peridotites and mylonites is contained within mineral matrices as opposed to fluid and melt inclusions [117]. Because mineral matrices may be more rugged than fluid inclusions, vacuum crushing of partially serpentinized Cayman peridotites may have released a smaller fraction of He relative to inclusion-hosted CH_4, resulting in elevated $CH_4/^3He$ ratios. Another process that may lower $CH_4/^3He$ ratios in vent fluids at Von Damm is the addition of mantle He from sources other than fluid

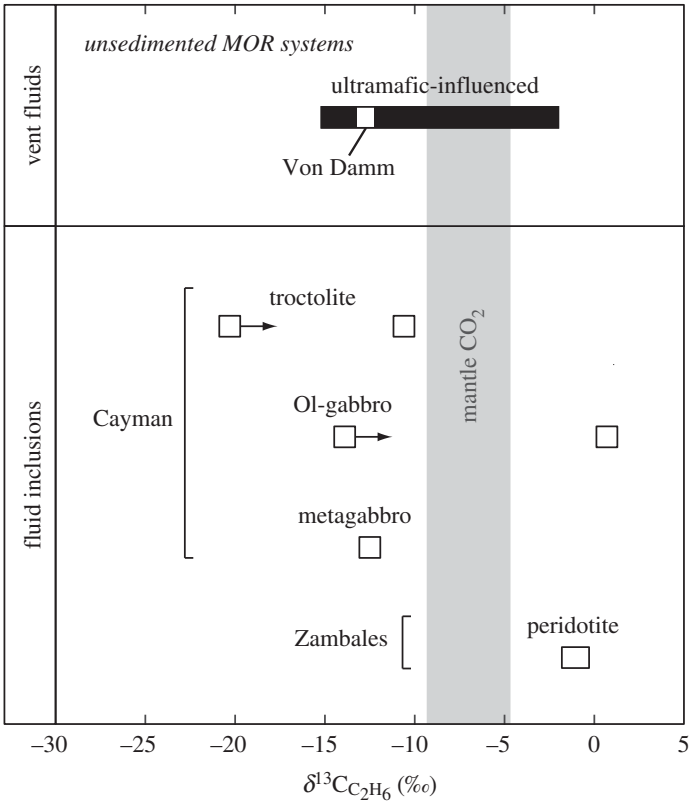

Figure 8. Ranges in carbon isotopic compositions of C_2H_6 from whole-rock samples in this study and ultramafic-influenced MOR vent fluids. Symbols with arrows denote minimum values due to C_2H_6 contamination detected from the crushing device (see text for details). The $\delta^{13}C$ value of dissolved C_2H_6 in Von Damm fluids (−12.7‰) is similar to $\delta^{13}C_{C_2H_6}$ values for most Cayman samples, with the exception of ALV 620-5-1. See text for discussion. Data are from [14,16,71,72,81,82].

inclusions, such as the crystallization of igneous rocks at depth. Since He in fluid inclusions is also mantle-derived, there would be no difference in the isotopic composition of He in rock samples and vent fluids.

Whole-rock hydrocarbon abundances in Cayman rock samples can be used to estimate the minimum water/rock mass ratios needed to account for the concentrations of dissolved CH_4 (2.81 mmol kg^{-1}) and C_2H_6 (639 nmol kg^{-1}) observed in endmember fluids at the Von Damm hydrothermal field [16]. Water/rock mass ratios were obtained by dividing the concentration of these species in the rock by their concentration in the endmember vent fluid. For these calculations, it was assumed that hydrocarbons are quantitatively leached during hydrothermal alteration by convecting fluids. Because the measured hydrocarbon abundances in Cayman rocks represent minimum values due to incomplete crushing of fluid inclusions, calculated water/rock ratios likely underestimate actual values. The CH_4 abundances in Cayman samples yield water/rock mass ratios of 0.002–0.11, while ratios calculated from C_2H_6 contents are approximately an order of magnitude higher and vary from 0.02 to 1.6 (table 4). Higher values calculated for C_2H_6 may reflect oxidative degradation of C_2H_6 in the fluids following extraction from the rock.

Water/rock mass ratios for Von Damm vent fluids can also be estimated using the abundance of inorganic trace elements. Based on the concentrations of Li and Rb in Von Damm vent fluids and Cayman rocks, water/rock mass ratios vary from 0.2 to 0.8 [34], consistent with the rock-dominated conditions indicated by hydrocarbon abundances in this study. The broader range of values calculated from hydrocarbon abundances and the extension to substantially lower values

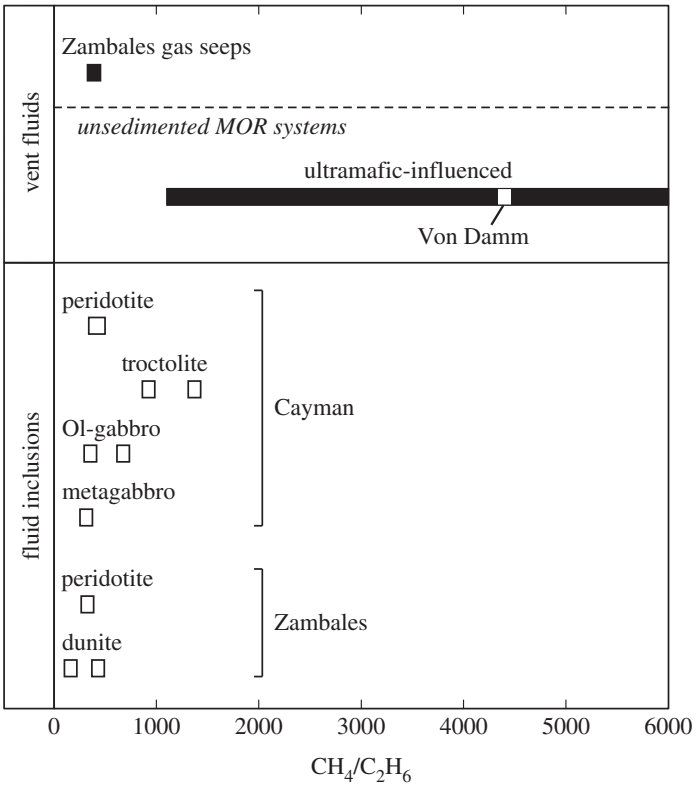

Figure 9. Range in CH_4/C_2H_6 ratios from whole-rock samples in this study, Zambales gas seeps and ultramafic-influenced MOR vent fluids. CH_4/C_2H_6 ratios in Zambales gas seeps are similar to measured ratios in serpentinized dunite and peridotite from the ophiolite. By contrast, CH_4/C_2H_6 ratios in Von Damm vent fluids are more than three times higher than those in Cayman rocks. See text for discussion. Data are from [13,14,16,17,81].

Table 4. Calculated water–rock (W/R) mass ratios needed to account for the concentrations of dissolved CH_4 and C_2H_6 in Von Damm hydrothermal fluids.

		W/R	
rock type	sample	CH_4	C_2H_6
gneissic metagabbro	ALV 620 3C	0.11	1.56
olivine gabbro	ALV 620 5-1	0.09	1.07
	ALV 624 5-1	0.03	0.21
troctolite	ALV 621 3-1	0.03	0.13
	ALV 623 3-2	0.03	0.07
peridotite	ALV 624 3-3	0.002	0.02
	ALV 624 6-2	0.004	0.03

may be attributed to alteration of the rock samples, which may have released trapped volatiles from fluid inclusions prior to their analysis. Peridotite samples, in particular, are more than 80–90% serpentinized according to visual estimates in thin section, suggesting that only a small fraction of secondary fluid inclusions have remained intact since their formation.

To examine the potential of fluid inclusions as a source of hydrocarbons in the Von Damm vent site, we estimate the CH_4 flux that can be supplied by the downward migration of cracks

that would enable convecting fluids to access inclusion-bearing rocks in the oceanic lithosphere. Seismic data by Harding *et al*. [33] suggest that hydrothermal circulation at Von Damm could be fueled by a cracking front mining heat from hot rocks beneath the Mt Dent oceanic core complex (e.g. [118]). Based on the flux of fluid estimated to vent at Von Damm (approx. 500 kg s^{-1}; [119]) and the concentration of dissolved CH_4 in endmember vent fluids (2.81 mmol l^{-1} [16]), release of CH_4 from fluid inclusion-bearing rocks would have to supply approximately 1 mol CH_4 s^{-1} to the endmember fluid. Assuming the crust contains approximately 1 mol CH_4 m^{-3} rock (corresponding to the most CH_4-rich rock sample measured in this study), such a CH_4 flux could be achieved by a cracking front that propagates downward at approximately 10 cm yr^{-1}, allowing the instantaneous release of CH_4 from the fluid inclusions to the hydrothermal fluid over a horizontal area of approximately 10 km^2. This area is consistent with the size of the seismically inferred heat source beneath Von Damm [33]. Furthermore, such a migration rate for the cracking front is within the bounds of rates estimated from models of thermal cracking in the oceanic lithosphere [118]. In addition, if we consider that hydrothermal circulation beneath Van Damm is occurring over the entire area of the Mt Dent oceanic core complex (of the order of 100 km^2), then the cracking front would only need to propagate downward at approximately 1 cm yr^{-1}. Propagation at this rate would roughly match the slip rate of the detachment fault that hosts the Von Damm field and allow the cracking front to remain stationary as the detachment fault exhumes deeper CH_4-bearing rocks that continuously replenish the supply of CH_4 available for leaching.

Dissolved hydrocarbons in vent fluids from unsedimented, ultramafic-influenced hydrothermal sites from a broad range of seafloor locations show remarkably similar concentrations and isotopic compositions to those in Von Damm vent fluids, despite the widely different subsurface temperatures, alteration histories and inorganic fluid chemistries of the hydrothermal sites (figures 7 and 8). For example, dissolved CH_4 exhibits a relatively narrow range in concentration from 0.5 to 3.5 mM, while dissolved C_2H_6 exhibits concentrations of 0.1–5.7 µM, with the majority of values falling between 0.6 and 1 µM for fluids from the Lost City, Rainbow, Logatchev, and even the mafic-hosted Lucky Strike hydrothermal fields [13,14,16,80,81,120]. $\delta^{13}C$ values vary from −17.8‰ to −6.1‰ in CH_4, and from −15.2‰ to −2.0‰ in C_2H_6 [13,14,16,80,81]. In addition, recent analyses of clumped methane isotopologues reveal similar apparent equilibrium temperatures of 310^{+53}_{-42}°C for a variety of ultramafic- and basalt-influenced seafloor hydrothermal systems [26]. In contrast to hydrocarbon abundances and isotopic compositions, measured vent fluid temperatures and $pH_{(25°C)}$ vary substantially from 96°C to 370°C and from 3.3 to 10.2, respectively. The similarity in hydrocarbon abundances and isotopic compositions at these vent fields with those observed at Von Damm suggests that leaching of volatiles from fluid inclusions during convective circulation of seawater-derived hydrothermal fluids may be a ubiquitous process.

Examination of figure 7 reveals that the range of $\delta^{13}C_{CH_4}$ values observed for CH_4 trapped in olivine-rich rocks from the Mid-Cayman Rise also shows a high degree of overlap with $\delta^{13}C_{CH_4}$ values measured for dissolved CH_4 in basalt-influenced hydrothermal systems. This similarity suggests that fluids hosted in mafic substrates may additionally be mining CH_4 from fluid inclusions in olivine-rich gabbroic rocks of oceanic layer 3 [20–23]. Variations of $CH_{4(aq)}$ concentrations measured in mafic-hosted hydrothermal systems may therefore reflect the abundance of olivine-rich gabbro interacting with convecting hydrothermal fluids along their flow path [22].

(ii) Zambales gas seeps

Abundant CH_4-rich fluid inclusions in olivine-rich rocks at the Zambales ophiolite represent a significant reservoir of hydrocarbons that may contribute to active gas seeps. Reduced gases venting from fractured, partially serpentinized ultramafic rock in the Zambales ophiolite contain up to 58.5 vol.% H_2 and up to 55 vol.% CH_4 [17,19,37,38]. Seep gases also contain elevated amounts of He (up to 6.9 ppm), C_2H_6 (up to 0.15 vol.%) and other C_{2+} hydrocarbons [17].

Estimated serpentinization temperatures for the Zambales ophiolite range from 350°C in the geological past to less than 100°C for present-day serpentinization [121,122].

Comparison of the relative abundances and isotopic compositions of volatiles in seep gases with those measured in olivine-rich rocks from the Zambales ophiolite reveals remarkable similarities. In particular, CH_4 gas collected from the Los Fuegos Eternos and Nagsasa seeps has average $\delta^{13}C_{CH_4}$ values of −7.0‰ and −5.6‰, respectively [17,19], which fall within the range of −12.4‰ to −2.8‰ measured for CH_4 hosted in fluid inclusions in serpentinized dunite and peridotite from the ophiolite (figure 7). Moreover, the range of CH_4/C_2H_6 ratios measured in serpentinized dunite and peridotite from Zambales during this study (163–431) overlaps with the range of CH_4/C_2H_6 ratios in Zambales gas seeps (325–457) [17] (figure 9). Average $^3He/^4He$ ratios of 3.0–5.6 R_a in serpentinized dunite and peridotite (table 3) also overlap with $^3He/^4He$ ratios of 4.03 ± 0.05 to 0.49 R_a at Los Fuegos Eternos and 4.35 R_a at Nagsasa gas seeps [17,19]. Similarly, the average $CH_4/^3He$ ratio in Zambales gas seeps ($1.6 \times 10^{10} \pm 0.2 \times 10^{10}$) [17] lies between measured $CH_4/^3He$ ratios in serpentinized samples ($8.06 \times 10^9 - 1.30 \times 10^{12}$) (figure 6). Overall, the abundance and isotopic compositions of hydrocarbons and He in ultramafic rocks presented here are remarkably similar to those of gases emanating from the Zambales ophiolite, suggesting that mining of fluid inclusion-hosted volatiles during alteration or fracturing of rocks may be a significant source of hydrocarbons at Zambales and possibly other continental gas seeps. For instance, available geochemical and radiometric constraints for the origin of CH_4 venting at Chimaera (Turkey), a serpentinite-hosted gas seep active for more than two millennia [123], are consistent with a fluid inclusion source. Abiotic CH_4 is interpreted to have formed at 120–140°C, which is significantly higher than the current temperature in the source rock [124], suggesting that CH_4 must have formed in the geological past when temperatures were higher. This interpretation is in keeping with radiocarbon constraints [123] and recent mass balance estimates indicating fluid inclusion abundances are sufficiently high to account for the source of abiotic CH_4 at Chimaera [23].

5. Conclusion

Lower crustal and upper mantle rocks at the Mid-Cayman Rise and the Zambales ophiolite contain appreciable quantities of CH_4 and C_2H_6 hosted in secondary fluid inclusions in olivine ± plagioclase ± clinopyroxene. Whole-rock CH_4 and C_2H_6 carbon isotopic compositions at the Mid-Cayman Rise are similar to the range observed in fluids venting at the Von Damm hydrothermal field and other ultramafic-influenced hydrothermal sites on the seafloor. Likewise, hydrocarbon and noble gas compositions in fluid inclusions in rocks from the Zambales ophiolite are strikingly similar to those of nearby gas seeps. These findings suggest that leaching of fluid inclusions by dissolution or fracturing of the rock may provide a significant contribution of hydrocarbons to hydrothermal fluids at Von Damm, gas seeps at Zambales, and possibly other ultramafic-influenced submarine and subaerial vent sites. It is also possible that CH_4 in basalt-hosted vent fluids may be derived from leaching of fluid inclusions in gabbroic rocks. While convecting seawater-derived fluids transport dissolved hydrocarbons to the seafloor, current evidence does not support their direct involvement in hydrocarbon production. Instead, CH_4 and C_{2+} alkanes appear to be formed in isolation from percolating fluids, such as in fluid inclusions where CO_2 reduction can take place over geologic time scales. It is proposed that CO_2 and H_2O become trapped in primary minerals as carbon-rich aqueous fluids circulate within cooling gabbroic and mantle rocks [23]. As temperatures decrease, entrapped CO_2 and H_2O react with their host minerals and undergo chemical re-equilibration. Reaction of olivine with H_2O below approximately 400°C is expected to generate H_2, thereby driving the reduction of CO_2 and resulting in the formation of secondary fluid inclusions enriched in CH_4, C_2H_6 and potentially other low molecular weight hydrocarbons. Subsequent extraction and transport of hydrocarbons to vent sites is mediated by convecting hydrothermal fluids. These findings have profound implications for models that describe the flux of carbon between the lithosphere and oceans as

well as its impact on microbial vent communities in seafloor and subseafloor environments that use reduced carbon species as a source of carbon and metabolic energy.

Data accessibility. The datasets supporting this article are included in tables and figures within this manuscript.

Authors' contributions. F.K. and J.S.S. conceived this study. All authors contributed to the conception and design of the method for extracting volatile carbon species from rock-hosted fluid inclusions. N.G.G. and S.P.S. collected the data, and all authors were involved in the interpretation of the acquired dataset. N.G.G. wrote the manuscript, with significant contributions to drafting and revision made by all authors. The final version of this manuscript has been approved by all authors.

Competing interests. We declare we have no competing interests.

Funding. This study was supported by the National Science Foundation through grant no. OCE-1634032 to F.K. and J.S.S. Additional financial support was provided by Louise Von Damm.

Acknowledgements. We thank Mark Kurz and Joshua Curtice for performing the helium isotopic measurements. We thank Karmina Aquino and Emmanuel Codillo for collecting samples from the Zambales ophiolite, and Karmina Aquino for performing some of the Raman analyses on the Zambales samples. This work benefited from fruitful discussions with Jean-Arthur Olive. Constructive reviews by Jeff Alt, associate editor Andrew McCaig and an anonymous reviewer greatly improved the manuscript.

References

1. Mottl MJ, Komor SC, Fryer P, Moyer CL. 2003 Deep-slab fluids fuel extremophilic Archaea on a Mariana forearc serpentinite mud volcano: Ocean Drilling Program Leg 195. *Geochem. Geophys. Geosyst.* **4**, 9009. (doi:10.1029/2003GC000588)
2. Schrenk MO, Kelley DS, Bolton SA, Baross JA. 2004 Low archaeal diversity linked to subseafloor geochemical processes at the Lost City Hydrothermal Field, Mid-Atlantic Ridge. *Environ. Microbiol.* **6**, 1086–1095. (doi:10.1111/j.1462-2920.2004.00650.x)
3. Schrenk MO, Brazelton WJ, Lang SQ. 2013 Serpentinization, carbon, and deep life. *Rev. Mineral. Geochem.* **75**, 575–606. (doi:10.2138/rmg.2013.75.18)
4. Curtis AC, Wheat CG, Fryer P, Moyer CL. 2013 Mariana forearc serpentinite mud volcanoes harbor novel communities of extremophilic Archaea. *Geomicrobiol. J.* **30**, 430–441. (doi:10.1080/01490451.2012.705226)
5. Quéméneur M *et al.* 2014 Spatial distribution of microbial communities in the shallow submarine alkaline hydrothermal field of the Prony Bay, New Caledonia. *Environ. Microbiol. Rep.* **6**, 665–674. (doi:10.1111/1758-2229.12184)
6. Sleep NH, Bird DK, Pope EC. 2011 Serpentinite and the dawn of life. *Phil. Trans. R. Soc. B* **366**, 2857–2869. (doi:10.1098/rstb.2011.0129)
7. Takai K, Nakamura K, Suzuki K, Inagaki F, Nealson KH, Kumagai H. 2006 Ultramafics-Hydrothermalism-Hydrogenesis-HyperSLiME (UltraH^3) linkage: a key insight into early microbial ecosystem in the Archean deep-sea hydrothermal systems. *Paleontol. Res.* **10**, 269–282. (doi:10.2517/prpsj.10.269)
8. Martin W, Baross J, Kelley D, Russell MJ. 2008 Hydrothermal vents and the origin of life. *Nat. Rev. Microbiol.* **6**, 805–814. (doi:10.1038/nrmicro1991)
9. Lane N, Allen JF, Martin W. 2010 How did LUCA make a living? Chemiosmosis in the origin of life. *Bioessays* **32**, 271–280. (doi:10.1002/bies.200900131)
10. Deamer D, Damer B. 2017 Can life begin on Enceladus? A perspective from hydrothermal chemistry. *Astrobiology* **17**, 834–839. (doi:10.1089/ast.2016.1610)
11. Waite JH *et al.* 2017 Cassini finds molecular hydrogen in the Enceladus plume: evidence for hydrothermal processes. *Science* **356**, 155–159. (doi:10.1126/science.aai8703)
12. Charlou JL, Donval JP. 1993 Hydrothermal methane venting between 12°N and 26°N along the Mid-Atlantic Ridge. *J. Geophys. Res.* **98**, 9625–9642. (doi:10.1029/92JB02047)
13. Charlou JL, Donval JP, Fouquet Y, Jean-Baptiste P, Holm N. 2002 Geochemistry of high H_2 and CH_4 vent fluids issuing from ultramafic rocks at the Rainbow hydrothermal field (36°14′N, MAR). *Chem. Geol.* **191**, 345–359. (doi:10.1016/S0009-2541(02)00134-1)
14. Proskurowski G, Lilley MD, Seewald JS, Früh-Green GL, Olson EJ, Lupton JE, Sylva SP, Kelley DS. 2008 Abiogenic hydrocarbon production at Lost City Hydrothermal Field. *Science* **319**, 604–607. (doi:10.1126/science.1151194)

15. Seyfried WE, Pester NJ, Tutolo BM, Ding K. 2015 The Lost City hydrothermal system: Constraints imposed by vent fluid chemistry and reaction path models on subseafloor heat and mass transfer processes. *Geochim. Cosmochim. Acta* **163**, 59–79. (doi:10.1016/j.gca.2015.04.040)
16. McDermott JM, Seewald JS, German CR, Sylva SP. 2015 Pathways for abiotic organic synthesis at submarine hydrothermal fields. *Proc. Natl Acad. Sci. USA* **112**, 7668–7672. (doi:10.1073/pnas.1506295112)
17. Abrajano TA, Sturchio NC, Bohlke JK, Lyon GL, Poreda RJ, Stevens CM. 1988 Methane-hydrogen gas seeps, Zambales Ophiolite, Philippines: deep or shallow origin? *Chem. Geol.* **71**, 211–222. (doi:10.1016/0009-2541(88)90116-7)
18. Hosgormez H, Etiope G, Yalçin MN. 2008 New evidence for a mixed inorganic and organic origin of the Olympic Chimaera fire (Turkey): a large onshore seepage of abiogenic gas. *Geofluids* **8**, 263–273. (doi:10.1111/j.1468-8123.2008.00226.x)
19. Vacquand C, Deville E, Beaumont V, Guyot F, Sissmann O, Pillot D, Arcilla C, Prinzhofer A. 2018 Reduced gas seepages in ophiolitic complexes: evidences for multiple origins of the H_2-CH_4-N_2 gas mixtures. *Geochim. Cosmochim. Acta* **223**, 437–461. (doi:10.1016/j.gca.2017.12.018)
20. Kelley DS. 1996 Methane-rich fluids in the oceanic crust. *J. Geophys. Res. Earth* **101**, 2943–2962. (doi:10.1029/95jb02252)
21. Kelley DS, Früh-Green GL. 1999 Abiogenic methane in deep-seated mid-ocean ridge environments: insights from stable isotope analyses. *J. Geophys. Res.* **104**, 10 439–10 460. (doi:10.1029/1999JB900058)
22. Kelley DS, Früh-Green GL. 2001 Volatile lines of descent in submarine plutonic environments: insights from stable isotope and fluid inclusion analyses. *Geochim. Cosmochim. Acta* **65**, 3325–3346. (doi:10.1016/S0016-7037(01)00667-6)
23. Klein F, Grozeva NG, Seewald JS. 2019 Abiotic methane synthesis and serpentinization in olivine-hosted fluid inclusions. *Proc. Natl Acad. Sci. USA* **116**, 17 666–17 672. (doi:10.1073/pnas.1907871116)
24. Kelley DS, Baross JA, Delaney JR. 2002 Volcanoes, fluids, and life at mid-ocean ridge spreading centers. *Annu. Rev. Earth Planet. Sci.* **30**, 385–491. (doi:10.1146/annurev.earth.30.091201.141331)
25. McCollom TM, Seewald JS. 2007 Abiotic synthesis of organic compounds in deep-sea hydrothermal environments. *Chem. Rev.* **107**, 382–401. (doi:10.1021/cr0503660)
26. Wang DT, Reeves EP, McDermott JM, Seewald JS, Ono S. 2018 Clumped isotopologue constraints on the origin of methane at seafloor hot springs. *Geochim. Cosmochim. Acta* **223**, 141–158. (doi:10.1016/j.gca.2017.11.030)
27. Stroup JB, Fox PJ. 1981 Geologic investigations in the Cayman Trough: evidence for thin oceanic crust along the Mid-Cayman Rise. *J. Geol.* **89**, 395–420. (doi:10.1086/628605)
28. Dimalanta CB, Salapare RC, Faustino-Eslava DV, Ramos NT, Queaño KL, Yumul GP, Yang TF. 2015 Post-emplacement history of the Zambales Ophiolite Complex: insights from petrography, geochronology and geochemistry of Neogene clastic rocks. *J. Asian Earth Sci.* **104**, 215–227. (doi:10.1016/j.jseaes.2014.07.021)
29. Ballard R *et al.* 1979 Geological and geophysical investigation of the Midcayman Rise spreading center: initial results and observations. In *Deep drilling results in the Atlantic Ocean: ocean crust* (eds M Talwani, CG Harrison, DE Hayes), pp. 66–93. Washington, DC: American Geophysical Union.
30. Hayman NW, Grindlay NR, Perfit MR, Mann P, Leroy S, De Lépinay BM. 2011 Oceanic core complex development at the ultraslow spreading Mid-Cayman Spreading Center. *Geochem. Geophys. Geosyst.* **12**, Q0AG02. (doi:10.1029/2010GC003240)
31. German CR *et al.* 2010 Diverse styles of submarine venting on the ultraslow spreading Mid-Cayman Rise. *Proc. Natl Acad. Sci. USA* **107**, 14 020–14 025. (doi:10.1073/pnas.1009205107)
32. Connelly DP *et al.* 2012 Hydrothermal vent fields and chemosynthetic biota on the world's deepest seafloor spreading centre. *Nat. Commun.* **3**, 620. (doi:10.1038/ncomms1636)
33. Harding JL, Van Avendonk HJA, Hayman NW, Grevemeyer I, Peirce C, Dannowski A. 2017 Magmatic-tectonic conditions for hydrothermal venting on an ultraslow-spread oceanic core complex. *Geology* **45**, 839–842. (doi:10.1130/G39045.1)

34. McDermott JM. 2015 Geochemistry of deep-sea hydrothermal vent fluids from the Mid-Cayman Rise, Caribbean Sea. PhD thesis, Massachusetts Institute of Technology, USA.
35. Malcolm FL. 1979 Petrography, mineral chemistry and microstructures of gabbros from the Mid-Cayman Rise spreading center. MS thesis, State University of New York at Albany, USA.
36. Elthon D. 1987 Petrology of gabbroic rocks from the Mid-Cayman rise spreading center. *J. Geophys. Res.* **92**, 658–682. (doi:10.1029/JB092iB01p00658)
37. Thayer TP. 1966 Serpentinization considered as a constant-volume metasomatic process. *Am. Mineral.* **51**, 685–710.
38. Abrajano TA, Sturchio NC, Kennedy BM, Lyon GL, Muehlenbachs K, Bohlke JK. 1990 Geochemistry of reduced gas related to serpentinization of the Zambales ophiolite, Philippines. *Appl. Geochem.* **5**, 625–630. (doi:10.1016/0883-2927(90)90060-I)
39. Yumul GP *et al.* In press. Slab rollback and microcontinent subduction in the evolution of the Zambales Ophiolite Complex (Philippines): a review. *Geosci. Front.* (doi:10.1016/j.gsf.2018.12.008)
40. Zhang J, Qiao S, Lu W, Hu Q, Chen S, Liu Y. 2016 An equation for determining methane densities in fluid inclusions with Raman shifts. *J. Geochem. Explor.* **171**, 20–28. (doi:10.1016/j.gexplo.2015.12.003)
41. Lu W, Chou IM, Burruss RC, Song Y. 2007 A unified equation for calculating methane vapor pressures in the CH_4-H_2O system with measured Raman shifts. *Geochim. Cosmochim. Acta* **71**, 3969–3978. (doi:10.1016/j.gca.2007.06.004)
42. Wopenka B, Pasteris JD. 1987 Raman intensities and detection limits of geochemically relevant gas mixtures for a laser Raman microprobe. *Anal. Chem.* **59**, 2165–2170. (doi:10.1021/ac00144a034)
43. Rosso KM, Bodnar RJ. 1995 Microthermometric and Raman spectroscopic detection limits of CO_2 in fluid inclusions and the Raman spectroscopic characterization of CO_2. *Geochim. Cosmochim. Acta* **59**, 3961–3975. (doi:10.1016/0016-7037(95)94441-H)
44. Lamadrid HM. 2016 Geochemistry of fluid-rock processes. PhD thesis, Virginia Polytechnic Institute and State University, USA.
45. Piperov NB, Penchev NP. 1973 A study on gas inclusions in minerals. Analysis of the gases from micro-inclusions in allanite. *Geochim. Cosmochim. Acta* **37**, 2075–2097. (doi:10.1016/0016-7037(73)90009-4)
46. Roedder E. 1984 *Fluid inclusions*. Washington, DC: Mineralogical Society of America.
47. Salvi S, Williams-Jones AE. 2003 Bulk analysis of volatiles in fluid inclusions. *Mineral. Assoc. Canada Short Course Ser.* **32**, 247–278.
48. Norman DI, Sawkins FJ. 1987 Analysis of volatiles in fluid inclusions by mass spectrometry. *Chem. Geol.* **61**, 1–10. (doi:10.1016/0009-2541(87)90020-9)
49. Norman DI, Harrison RW, Andres CB. 1991 Geology and geochemical analysis of mineralizing fluids at the St. Cloud and U.S. Treasury Mines, Chloride Mining District, New Mexico. *J. Geochem. Explor.* **42**, 61–89. (doi:10.1016/0375-6742(91)90060-8)
50. Abell PI, Draffan CH, Eglinton G, Hayes JM, Maxwell JR, Pillinger CT. 1970 Organic analysis of the returned Apollo 11 lunar sample. *Proc. Apollo 11 Lunar Sci. Conf.* **2**, 1757–1773.
51. Andrawes F, Holzer G, Roedder E, Gibson EKJ, Oro J. 1984 Gas chromatographic analysis of volatiles in fluid and gas inclusions. *J. Chromatogr.* **302**, 181–193. (doi:10.1016/S0021-9673(01)89010-5)
52. Andrawes FF, Gibson EKJ. 1979 Release and analysis of gases from geological samples. *Am. Mineral.* **64**, 453–463.
53. Welhan JA. 1988 Methane and hydrogen in mid-ocean-ridge basalt glasses: Analysis by vacuum crushing. *Can. J. Earth Sci.* **25**, 38–48. (doi:10.1139/e88-004)
54. Roedder E. 1972 Composition of fluid inclusions. *U.S. Geol. Surv. Prof. Pap.* **440**, 1–164. (doi:10.3133/pp440JJ)
55. Kurz MD, Gurney JJ, Jenkins WJ, Lott DE. 1987 Helium isotopic variability within single diamonds from the Orapa kimberlite pipe. *Earth Planet. Sci. Lett.* **86**, 57–68. (doi:10.1016/0012-821X(87)90188-9)

56. Kurz MD, Curtice J, Lott DE, Solow A. 2004 Rapid helium isotopic variability in Mauna Kea shield lavas from the Hawaiian Scientific Drilling Project. *Geochem. Geophys. Geosyst.* **5**, Q04G14. (doi:10.1029/2002GC000439)
57. Kurz MD, Jenkins WJ. 1981 The distribution of helium in oceanic basalt glasses. *Earth Planet. Sci. Lett.* **53**, 41–54. (doi:10.1016/0012-821X(81)90024-8)
58. Allègre CJ, Staudacher T, Sarda P, Kurz MD. 1983 Constraints on evolution of Earth's mantle from rare gas systematics. *Nature* **303**, 762–766. (doi:10.1038/303762a0)
59. Hiyagon H, Ozima M, Marty B, Zashu S, Sakai H. 1992 Noble gases in submarine glasses from mid-oceanic ridges and Loihi seamount: constraints on the early history of the Earth. *Geochim. Cosmochim. Acta* **56**, 1301–1316. (doi:10.1016/0016-7037(92)90063-O)
60. Harper D. 1985 Tectonics of slow spreading mid-ocean ridges and consequences of a variable depth to the brittle/ductile transition. *Tectonics* **4**, 395–409. (doi:10.1029/TC004i004p00395)
61. Jones MR *et al.* 2019 New constraints on mantle carbon from Mid-Atlantic Ridge popping rocks. *Earth Planet. Sci. Lett.* **511**, 67–75. (doi:10.1016/j.epsl.2019.01.019)
62. Allen DE, Seyfried WEJ. 2003 Compositional controls on vent fluids from ultramafic-hosted hydrothermal systems at mid-ocean ridges: An experimental study at 400°C, 500 bars. *Geochim. Cosmochim. Acta* **67**, 1531–1542. (doi:10.1016/S0016-7037(02)01173-0)
63. Klein F, Bach W, McCollom TM. 2013 Compositional controls on hydrogen generation during serpentinization of ultramafic rocks. *Lithos* **178**, 55–69. (doi:10.1016/j.lithos.2013.03.008)
64. McCollom TM, Klein F, Robbins M, Moskowitz B, Berquó TS, Jöns N, Bach W, Templeton A. 2016 Temperature trends for reaction rates, hydrogen generation, and partitioning of iron during experimental serpentinization of olivine. *Geochim. Cosmochim. Acta* **181**, 175–200. (doi:10.1016/j.gca.2016.03.002)
65. Shock EL. 1990 Geochemical constraints on the origin of organic compounds in hydrothermal systems. *Orig. Life Evol. Biosph.* **20**, 331–367. (doi:10.1007/BF01808115)
66. Früh-Green GL, Connolly JAD, Plas A, Kelley DS, Grobety B. 2004 Serpentinization of oceanic peridotites: implications for geochemical cycles and biological activity. In *The subseafloor biosphere at mid-ocean ridges* (eds WSD Wilcock, EF Delong, DS Kelley, JA Baross, S Craig Cary), pp. 119–136. Washington, DC: American Geophysical Union.
67. Klein F, McCollom TM. 2013 From serpentinization to carbonation: new insights from a CO_2 injection experiment. *Earth Planet. Sci. Lett.* **379**, 137–145. (doi:10.1016/j.epsl.2013.08.017)
68. Hentscher M. 2012 Thermodynamic investigations of microbial metabolism and abiotic organic synthesis in seafloor hydrothermal systems. PhD thesis, University of Bremen.
69. Evans BW, Yang H. 1998 Fe-Mg order-disorder in tremolite-actinolite-ferro-actinolite at ambient and high temperature. *Am. Mineral.* **83**, 458–475. (doi:10.2138/am-1998-5-606)
70. Kurz MD, Moreira M, Curtice J, Lott DE, Mahoney JJ, Sinton JM. 2005 Correlated helium, neon, and melt production on the super-fast spreading East Pacific Rise near 17°S. *Earth Planet. Sci. Lett.* **232**, 125–142. (doi:10.1016/j.epsl.2005.01.005)
71. Des Marais DJ, Moore JG. 1984 Carbon and its isotopes in mid-oceanic basaltic glasses. *Earth Planet. Sci. Lett.* **69**, 43–57. (doi:10.1016/0012-821X(84)90073-6)
72. Sakai H, Des Marais DJ, Ueda A, Moore JG. 1984 Concentrations and isotope ratios of carbon, nitrogen and sulfur in ocean-floor basalts. *Geochim. Cosmochim. Acta* **48**, 2433–2441. (doi:10.1016/0016-7037(84)90295-3)
73. Charlou JL, Donval JP, Douville E, Jean-Baptiste P, Radford-Knoery J, Fouquet Y, Dapoigny A, Stievenard M. 2000 Compared geochemical signatures and the evolution of Menez Gwen (35°50′N) and Lucky Strike (37°17′N) hydrothermal fluids, south of the Azores Triple Junction on the Mid-Atlantic Ridge. *Chem. Geol.* **171**, 49–75. (doi:10.1016/S0009-2541(00)00244-8)
74. Gamo T *et al.* 2001 Chemical characteristics of newly discovered black smoker fluids and associated hydrothermal plumes at the Rodriguez Triple Junction, Central Indian Ridge. *Earth Planet. Sci. Lett.* **193**, 371–379. (doi:10.1016/S0012-821X(01)00511-8)
75. Takai K, Gamo T, Tsunogai U, Nakayama N, Hirayama H, Nealson KH, Horikoshi K. 2004 Geochemical and microbiological evidence for a hydrogen-based, hyperthermophilic subsurface lithoautotrophic microbial ecosystem (HyperSLiME) beneath an active deep-sea hydrothermal field. *Extremophiles* **8**, 269–282. (doi:10.1007/s00792-004-0386-3)

76. Charlou JL, Fouquet Y, Donval JP, Auzende JM, Jean-Baptiste P, Stievenard M, Michel S. 1996 Mineral and gas chemistry of hydrothermal fluids on an ultrafast spreading ridge: East Pacific Rise, 17° to 19°S (Naudur cruise, 1993) phase separation processes controlled by volcanic and tectonic activity. *J. Geophys. Res.* **101**, 15 899–15 919. (doi:10.1029/96JB00880)
77. Merlivat L, Pineau F, Javoy M. 1987 Hydrothermal vent waters at 13°N on the East Pacific Rise: isotopic composition and gas concentration. *Earth Planet. Sci. Lett.* **84**, 100–108. (doi:10.1016/0012-821X(87)90180-4)
78. Evans WC, White LD, Rapp JB. 1988 Geochemistry of some gases in hydrothermal fluids from the southern Juan de Fuca Ridge. *J. Geophys. Res.* **93**, 15 305–15 313. (doi:10.1029/JB093iB12p15305)
79. Welhan JA, Craig H. 1983 Methane, hydrogen and helium in hydrothermal fluids at 21°N on the East Pacific Rise. In *Hydrothermal processes at seafloor spreading centers* (eds PA Rona, K Boström, L Laubier, KL Smith), pp. 391–409. Boston, MA: Springer.
80. Kelley DS *et al.* 2005 A serpentinite-hosted ecosystem: the Lost City hydrothermal field. *Science* **307**, 1428–1434. (doi:10.1126/science.1102556)
81. Charlou JL, Donval JP, Konn C, Ondréas H, Fouquet Y, Jean-Baptiste P, Fourré E. 2010 High production and fluxes of H_2 and CH_4 and evidence of abiotic hydrocarbon synthesis by serpentinization in ultramafic-hosted hydrothermal systems on the Mid-Atlantic Ridge. In *Diversity of hydrothermal systems on slow spreading ocean ridges* (eds PA Rona, CW Devey, J Dyment, BJ Murton), pp. 265–296. Washington, DC: American Geophysical Union.
82. Blank JG, Delaney JR, Des Marais DJ. 1993 The concentration and isotopic composition of carbon in basaltic glasses from the Juan de Fuca Ridge, Pacific Ocean. *Geochim. Cosmochim. Acta* **57**, 875–887. (doi:10.1016/0016-7037(93)90175-V)
83. McCollom TM, Seewald JS. 2006 Carbon isotope composition of organic compounds produced by abiotic synthesis under hydrothermal conditions. *Earth Planet. Sci. Lett.* **243**, 74–84. (doi:10.1016/j.epsl.2006.01.027)
84. Horita J, Berndt ME. 1999 Abiogenic methane formation and isotopic fractionation under hydrothermal conditions. *Science* **2**, 1055–1057. (doi:10.1126/science.285.5430.1055)
85. Sherwood Lollar B, Lacrampe-Couloume G, Voglesonger K, Onstott TC, Pratt LM, Slater GF. 2008 Isotopic signatures of CH_4 and higher hydrocarbon gases from Precambrian Shield sites: a model for abiogenic polymerization of hydrocarbons. *Geochim. Cosmochim. Acta* **72**, 4778–4795. (doi:10.1016/j.gca.2008.07.004)
86. Etiope G, Sherwood Lollar B. 2013 Abiotic methane production on earth. *Rev. Geophys.* **51**, 276–299. (doi:10.1002/rog.20011)
87. Pineau F, Mathez EA. 1990 Carbon isotopes in xenoliths from the Hualalai Volcano, Hawaii, and the generation of isotopic variability. *Geochim. Cosmochim. Acta* **54**, 217–227. (doi:10.1016/0016-7037(90)90209-4)
88. Tingle TN, Hochella MF, Becker CH, Malhotra R. 1990 Organic compounds on crack surfaces in olivine from San Carlos, Arizona and Hualalai Volcano, Hawaii. *Geochim. Cosmochim. Acta* **54**, 477–485. (doi:10.1016/0016-7037(90)90337-K)
89. Tingle TN, Mathez EA, Hochella Jr. MF. 1991 Carbonaceous matter in peridotites and basalts studied by XPS, SALI, and LEED. *Geochim. Cosmochim. Acta* **55**, 1345–1352. (doi:10.1016/0016-7037(91)90312-S)
90. Mathez EA. 1987 Carbonaceous matter in mantle xenoliths: composition and relevance to the isotopes. *Geochim. Cosmochim. Acta* **51**, 2339–2347. (doi:10.1016/0016-7037(87)90288-2)
91. Sugisaki R, Mimura K. 1994 Mantle hydrocarbons: abiotic or biotic? *Geochim. Cosmochim. Acta* **58**, 2527–2542. (doi:10.1016/0016-7037(94)90029-9)
92. Mathez EA, Delaney JR. 1981 The nature and distribution of carbon in submarine basalts and peridotite nodules. *Earth Planet. Sci. Lett.* **56**, 217–232. (doi:10.1016/0012-821X(81)90129-1)
93. Deines P. 2002 The carbon isotope geochemistry of mantle xenoliths. *Earth Sci. Rev.* **58**, 247–278. (doi:10.1016/S0012-8252(02)00064-8)
94. Delacour A, Früh-Green GL, Bernasconi SM, Schaeffer P, Kelley DS. 2008 Carbon geochemistry of serpentinites in the Lost City Hydrothermal System (30°N, MAR). *Geochim. Cosmochim. Acta* **72**, 3681–3702. (doi:10.1016/j.gca.2008.04.039)

95. Shilobreeva S, Martinez I, Busigny V, Agrinier P, Laverne C. 2011 Insights into C and H storage in the altered oceanic crust: Results from ODP/IODP Hole 1256D. *Geochim. Cosmochim. Acta* **75**, 2237–2255. (doi:10.1016/j.gca.2010.11.027)
96. Schwarzenbach EM, Früh-Green GL, Bernasconi SM, Alt JC, Plas A. 2013 Serpentinization and carbon sequestration: a study of two ancient peridotite-hosted hydrothermal systems. *Chem. Geol.* **351**, 115–133. (doi:10.1016/j.chemgeo.2013.05.016)
97. Klein F, Humphris SE, Guo W, Schubotz F, Schwarzenbach EM, Orsi WD. 2015 Fluid mixing and the deep biosphere of a fossil Lost City-type hydrothermal system at the Iberia Margin. *Proc. Natl Acad. Sci. USA* **112**, 12 036–12 041. (doi:10.1073/pnas.1504674112)
98. McCollom TM, Seewald JS. 2001 A reassessment of the potential for reduction of dissolved CO_2 to hydrocarbons during serpentinization of olivine. *Geochim. Cosmochim. Acta* **65**, 3769–3778. (doi:10.1016/S0016-7037(01)00655-X)
99. McCollom TM, Seewald JS. 2003 Experimental constraints on the hydrothermal reactivity of organic acids and acid anions: I. Formic acid and formate. *Geochim. Cosmochim. Acta* **67**, 3625–3644. (doi:10.1016/S0016-7037(03)00136-4)
100. Seewald JS, Zolotov MY, McCollom T. 2006 Experimental investigation of single carbon compounds under hydrothermal conditions. *Geochim. Cosmochim. Acta* **70**, 446–460. (doi:10.1016/j.gca.2005.09.002)
101. Grozeva NG, Klein F, Seewald JS, Sylva SP. 2017 Experimental study of carbonate formation in oceanic peridotite. *Geochim. Cosmochim. Acta* **199**, 264–286. (doi:10.1016/j.gca.2016.10.052)
102. Kadko D, Butterfield DA. 1998 The relationship of hydrothermal fluid composition and crustal residence time to maturity of vent fields on the Juan de Fuca Ridge. *Geochim. Cosmochim. Acta* **62**, 1521–1533. (doi:10.1016/S0016-7037(98)00088-X)
103. Kadko D, Moore W. 1988 Radiochemical constraints on the crustal residence time of submarine hydrothermal fluids: Endeavor Ridge. *Geochim. Cosmochim. Acta* **52**, 659–668. (doi:10.1016/0016-7037(88)90328-6)
104. Elderfield H, Wheat CG, Mottl MJ, Monnin C, Spiro B. 1999 Fluid and geochemical transport through oceanic crust: a transect across the eastern flank of the Juan de Fuca Ridge. *Earth Planet. Sci. Lett.* **172**, 151–165. (doi:10.1016/S0012-821X(99)00191-0)
105. Walker BD, McCarthy MD, Fisher AT, Guilderson TP. 2008 Dissolved inorganic carbon isotopic composition of low-temperature axial and ridge-flank hydrothermal fluids of the Juan de Fuca Ridge. *Mar. Chem.* **108**, 123–136. (doi:10.1016/j.marchem.2007.11.002)
106. Wheat CG, Fisher AT. 2008 Massive, low-temperature hydrothermal flow from a basaltic outcrop on 23 Ma seafloor of the Cocos Plate: chemical constraints and implications. *Geochem., Geophys. Geosyst.* **9**, Q12O14. (doi:10.1029/2008GC002136)
107. Grimes CB, John BE, Cheadle MJ, Wooden JL. 2008 Protracted construction of gabbroic crust at a slow spreading ridge: constraints from $^{206}Pb/^{238}U$ zircon ages from Atlantis Massif and IODP Hole U1309D (30°N, MAR). *Geochem. Geophys. Geosyst.* **9**, Q08012. (doi:10.1029/2008GC002063)
108. Baines AG, Cheadle MJ, John BE, Grimes CB, Schwartz JJ, Wooden JL. 2009 SHRIMP Pb/U zircon ages constrain gabbroic crustal accretion at Atlantis Bank on the ultraslow-spreading Southwest Indian Ridge. *Earth Planet. Sci. Lett.* **287**, 540–550. (doi:10.1016/j.epsl.2009.09.002)
109. John BE, Foster DA, Murphy JM, Cheadle MJ, Baines AG, Fanning CM, Copeland P. 2004 Determining the cooling history of in situ lower oceanic crust-Atlantis Bank, SW Indian Ridge. *Earth Planet. Sci. Lett.* **222**, 145–160. (doi:10.1016/j.epsl.2004.02.014)
110. Schwartz JJ, John BE, Cheadle MJ, Reiners PW, Baines AG. 2009 Cooling history of Atlantis Bank oceanic core complex: evidence for hydrothermal activity 2.6 Ma off axis. *Geochem. Geophys. Geosyst.* **10**, Q08020. (doi:10.1029/2009GC002466)
111. Grimes CB, Cheadle MJ, John BE, Reiners PW, Wooden JL. 2011 Cooling rates and the depth of detachment faulting at oceanic core complexes: evidence from zircon Pb/U and (U-Th)/He ages. *Geochem. Geophys. Geosyst.* **12**, Q0AG01. (doi:10.1029/2010GC003391)
112. Buck WR, Lavier LL, Poliakov ANB. 2005 Modes of faulting at mid-ocean ridges. *Nature* **434**, 719–723. (doi:10.1038/nature03358)
113. Schoolmeesters N, Cheadle MJ, John BE, Reiners PW, Gee J, Grimes CB. 2012 The cooling history and the depth of detachment faulting at the Atlantis Massif oceanic core complex. *Geochem. Geophys. Geosyst.* **13**, Q0AG12. (doi:10.1029/2012GC004314)

114. DeMartin BJ, Sohn RA, Canales JP, Humphris SE. 2007 Kinematics and geometry of active detachment faulting beneath the Trans-Atlantic geotraverse (TAG) hydrothermal field on the Mid-Atlantic Ridge. *Geology* **35**, 711–714. (doi:10.1130/G23718A.1)
115. Parnell-Turner R, Sohn RA, Peirce C, Reston TJ, MacLeod CJ, Searle RC, Simão NM. 2017 Oceanic detachment faults generate compression in extension. *Geology* **45**, 923–926. (doi:10.1130/G39232.1)
116. Seewald JS. 2001 Aqueous geochemistry of low molecular weight hydrocarbons at elevated temperatures and pressures: constraints from mineral buffered laboratory experiments. *Geochim. Cosmochim. Acta* **65**, 1641–1664. (doi:10.1016/S0016-7037(01)00544-0)
117. Kurz MD, Warren JM, Curtice J. 2009 Mantle deformation and noble gases: helium and neon in oceanic mylonites. *Chem. Geol.* **266**, 10–18. (doi:10.1016/j.chemgeo.2008.12.018)
118. Olive JA, Crone TJ. 2018 Smoke without fire: How long can thermal cracking sustain hydrothermal circulation in the absence of magmatic heat? *J. Geophys. Res. Solid Earth* **123**, 4561–4581, (doi:10.1029/2017JB014900)
119. Hodgkinson MRS, Webber AP, Roberts S, Mills RA, Connelly DP, Murton BJ. 2015 Talc-dominated seafloor deposits reveal a new class of hydrothermal system. *Nat. Commun.* **6**, 10150. (doi:10.1038/ncomms10150)
120. Schmidt K, Koschinsky A, Garbe-Schönberg D, de Carvalho LM, Seifert R. 2007 Geochemistry of hydrothermal fluids from the ultramafic-hosted Logatchev hydrothermal field, 15°N on the Mid-Atlantic Ridge: temporal and spatial investigation. *Chem. Geol.* **242**, 1–21. (doi:10.1016/j.chemgeo.2007.01.023)
121. Abrajano TA. 1984 Igneous petrology and low temperature geochemistry of the Acoje massif, Zambales Ophiolite, Philippines: mineralogical, isotopic, and mixed-volatile equilibria. PhD thesis, Washington University in St. Louis, USA.
122. Sturchio NC, Abrajano TA, Murowchick JB, Muehlenbachs K. 1989 Serpentinization of the Acoje massif, Zambales ophiolite, Philippines: hydrogen and oxygen isotope geochemistry. *Tectonophysics* **168**, 101–107. (doi:10.1016/0040-1951(89)90370-3)
123. Etiope G, Schoell M. 2014 Abiotic gas: atypical, but not rare. *Elements* **10**, 291–296. (doi:10.2113/gselements.10.4.291)
124. Young ED *et al.* 2017 The relative abundances of resolved $^{12}CH_2D_2$ and $^{13}CH_3D$ and mechanisms controlling isotopic bond ordering in abiotic and biotic methane gases. *Geochim. Cosmochim. Acta* **203**, 235–264. (doi:10.1016/J.GCA.2016.12.041)